Age of air from in situ trace gas measurements: Insights from a new technique

Eric A. Ray[1,2], Fred L. Moore[1,3], Hella Garny[4,5], Eric J. Hintsa[1,3], Bradley D. Hall[3], Geoff S. Dutton[1,3], David Nance[1,3], James W. Elkins[3,6], Steven C. Wofsy[7], Jasna Pittman[7], Bruce Daube[7], Bianca C. Baier[3], Jianghanyang Li[8,9] and Colm Sweeney[3]

[1]Cooperative Institute for Research in Environmental Sciences, University of Colorado Boulder, CO, USA
[2]NOAA Chemical Sciences Laboratory, Boulder, CO, USA
[3]NOAA Global Monitoring Laboratory, Boulder, CO, USA
[4]Deutsches Zentrum für Luft- und Raumfahrt (DLR), Institut für Physik der Atmosphäre, Oberpfaffenhofen, Germany
[5]Ludwig-Maximilians-University Munich, Meteorological Institute, Munich, Germany
[6]Retired
[7]Department of Earth and Planetary Sciences, Harvard University, Cambridge, MA, USA
[8]Department of Atmospheric and Oceanic Sciences, CU Boulder, CO, USA
[9]Institute of Arctic and Alpine Research, CU Boulder, CO, USA

Correspondence to: Eric A. Ray, eric.ray@noaa.gov

Abstract. The age of air is an important transport diagnostic that can be derived from trace gas measurements and compared to global chemistry climate model output. We describe a new technique to calculate the age of air, measuring transport times from the Earth's surface to any location in the atmosphere based on simultaneous *in situ* measurements of multiple key long-lived trace gases. The primary benefits of this new technique include (1) optimized ages of air consistent with simultaneously measured SF_6 and CO_2, (2) age of air from the upper troposphere through the stratosphere, (3) estimates of the second moment of age spectra that have not been well constrained from measurements and (4) flexibility to be used with measurements across multiple instruments, platforms and decades. We demonstrate the technique on aircraft and balloon measurements from the 1990s, the last period of extensive stratospheric *in situ* sampling, and several recent missions from the 2020s, and compare the results with previously published and modeled values.

1 Introduction

Age of air has been used as an observationally-based diagnostic of atmospheric transport for a number of decades (e.g., Bischof et al., 1985; Woodbridge et al., 1995; Schoeberl et al., 2005; Engel et al., 2017; Ray et al., 2022). The

stratospheric age of air is controlled by both the residual mean circulation and quasi-horizontal mixing (Waugh and Hall, 2002; Ploeger et al., 2014) and thus can give unique insight into these primary transport processes that govern the distribution of radiatively and chemically important trace gases in the stratosphere. An ideal trace gas to calculate mean ages, the first moment of the age spectra, would have a linear growth rate and be essentially inert in the atmosphere. Since this ideal trace gas does not exist in nature, we use measured trace gases with long lifetimes and photochemical production or loss that can be accounted for and are in growth or decay. Most calculations of mean ages from *in situ* measurements have been based on a single trace gas with these characteristics, such as carbon dioxide (CO_2) (Bischof et al., 1985; Schmidt and Khedim, 1991; Woodbridge et al., 1995; Boering et al., 1996; Andrews et al., 2001) or sulfur hexafluoride (SF_6) (Volk et al.,1997; Engel et al., 2008). In the case of CO_2, simultaneous measurements of methane (CH_4) and nitrous oxide (N_2O) are needed to adjust for CO_2 production and to account for the complication of interpreting the seasonal cycle of CO_2 for the youngest ages (Boering et al., 1996; Andrews et al., 2001).

Each age of air calculation technique from a single trace gas has complications that lead to uncertainty in the age values. These complications include accurately accounting for photochemical production or loss of a trace gas, such as the mesospheric loss of SF_6 (Loeffel et al., 2022; Garny et al., 2024), or accurately characterizing the boundary condition of a trace gas, whether at the tropopause or the Earth's surface (e.g., Engel et al., 2008). Comparisons between mean age estimates from different trace gas measurements have been difficult due to the sparsity of simultaneous measurements of multiple age-of-air species, but when available the differences have been shown to be significant (e.g., Leedham Elvidge et al., 2018). This uncertainty from the measurement-based estimates is compounded by the large disagreement among chemistry-climate model (CCM) and reanalysis-based age of air (Chabrillat et al., 2018; Ploeger et al., 2019; Abalos et al., 2021) that leaves us with a significant gap in our quantification of the stratospheric age of air and thus also the important processes that determine it as well as their changes over time.

One possibility to improve the calculation of age of air from observations is with the use of multiple simultaneous or near simultaneously measured trace gases, which has been shown previously to have potential for calculating age of air with more fidelity compared to estimates from a single trace gas (e.g., Schoeberl et al., 2005; Ehhalt et al., 2007; Boenisch et al., 2009; Ray et al., 2022). The main advantage of using multiple trace gases is to reduce the uncertainties or biases caused by the characteristics of a single trace gas to define the age of air (e.g. the seasonal cycle of CO_2). A detail of these techniques is that each trace gas does not contribute equally to the determination of age of air, that is, only the longest-lived trace gases that are in growth (or decay) can quantify the range of ages in the stratosphere (Podglajen and Ploeger, 2019). Thus, trace gases such as CO_2, SF_6 and carbon tetrafluoride (CF_4), referred to as primary age trace gases, can be used to make independent estimates of the age, while shorter lived trace gases such as trichlorofluoromethane (CFC-11) or chloromethane (CH_3Cl) can be used only in addition to the longer-lived trace gases to give information about the shortest ages (weeks to months) typically found in the tropopause region (Ray et al., 2022).

The main disadvantages of using multiple trace gases in an age of air calculation are (1) the previously mentioned

75   sparsity of simultaneous measurements of the most suitable trace gases and (2) the detailed knowledge of boundary

conditions for each trace gas that are required for accurate age of air estimates. The sparsity of simultaneous

measurements is due to the different measurement techniques and sampling frequency for each trace gas, as well as

aircraft and balloon payloads that may not have included multiple instruments suitable for age-of-air trace gas

measurements. The knowledge of boundary conditions for many trace gases, especially either at the tropical surface

80   or tropopause, is limited by whether long term measurements by a network are available. These disadvantages have

confined age of air estimates with multiple tracers to limited times and locations (e.g. Luo et al., 2018; Ray et al.,

2022).

In this work we demonstrate a new optimization technique to obtain mean age of air, along with several other

85   transport diagnostics, from simultaneous measurements of multiple primary age trace gases. The technique is

applicable to any primary age trace gases and we use the examples of SF_6 and CO_2 here. This method is somewhat

of a hybrid between the traditional single trace gas mean age estimates and the multiple trace gas techniques,

especially the work of Boenisch et al. (2009). As in Boenisch et al. (2009) and Ray et al. (2022), we leverage

additional information beyond mean age obtained in the optimization of a solution from multiple trace gases. Also,

90   similar to those two studies, we use the Earth's surface as the boundary condition of age of air, since that is where

we have long-term measurements of each trace gas. This method allows for transport characteristics of the upper

troposphere and tropopause region to be included as well as information about the latitudinal surface source regions.

The use of SF_6 measurements in the technique presented here is made possible by new estimates of SF_6 mesospheric

loss (Garny et al., 2024) that are used in the optimization.

95

This paper focuses on the details of the new technique with some example results using measurements from the

1990s and more recently from the 2020s. A follow up paper will explore the differences in the age of air between

these two time periods. The next section describes the data used in the examples shown in here. Section 3 describes

the method and Sect. 4 shows some results based on *in situ* measurements.

100

2 Data

For the stratospheric data in this study, we use aircraft and balloon-based *in situ* measurements of SF_6 (Elkins et al.,

1996; Moore et al., 2003; Hintsa et al., 2021), CO_2 (Daube et al., 2002), CH_4 and N_2O (Webster et al., 1994, 2001;

105   Loewenstein et al., 2002) as well as balloon-based AirCore measurements of these four species (Baier et al., 2021;

Li et al., 2023). AirCores (or larger-volume, dual-dimension StratoCores) are measured by two different analytical

systems for trace gas species used in this analysis: by cavity ring-down spectrometry for CO_2, N_2O and CH_4, and by

a gas chromatograph coupled with an electron capture detector for SF_6 and N_2O (Li et al., 2023). We use

measurements from both the 1990s, the last time period of extensive stratospheric *in situ* sampling of age of air trace

110   gases above 16 km, and from several recent missions and routine measurements in the 2020s. The 1990s ER-2 aircraft missions include ASHOE-MAESA (1994), STRAT (1995-96), POLARIS (1997) and SOLVE (1999-2000) and balloon-based data from Observations of the Middle Stratosphere (OMS, 1996-2000). The 2020s airborne missions include the Dynamics and Chemistry of the Summer Stratosphere (DCOTSS, 2021-22, ER-2) and Stratospheric Aerosol, processes, Budget and Radiative Effects (SABRE, 2023, WB-57) aircraft campaigns as well

115   as routine AirCore sampling (2021-24, Karion et al., 2010; Baier et al., 2021; Li et al., 2023). Mean ages have been previously calculated from the measurements in the 1990s, which allows us to compare the results shown here with those values (Volk et al., 1997; Andrews et al., 2001), but no mean ages have yet been published based on the 2020s measurements.

120   In order to use the method described in the next section we need simultaneous measurements of several trace gases, which has been exceptionally rare even when the aircraft or balloon platform carried all of the required instruments, due to different sampling and calibration timing. *In situ* CO_2, as well as CH_4 and N_2O, have typically been measured at ~1-5 second resolution, while SF_6 has been measured at ~1-2 minute resolution. In order to markedly increase the number of sample times with simultaneous mole fractions of the four trace gases considered here, we

125   interpolated in time across measurement gaps of up to 100 seconds in one or more of the trace gases. This time gap corresponds to a horizontal distance of ~20 km at typical ER-2 aircraft flying speeds and a vertical distance of ~0.3-0.5 km for typical balloon ascent and descent rates. For long-lived trace gases in the stratosphere such as those considered here, variability over the interpolated spatial scales is sufficiently small in almost all cases to not significantly affect the results.

130

A critical part of the method is to have latitudinally and time-varying surface mole fractions of the key trace gases listed above. For the surface boundary condition of each trace gas, we use the NOAA Greenhouse Gas Marine Boundary Layer (MBL) Reference product (https://gml.noaa.gov/ccgg/mbl/index.html; Lan et al., 2023) when available. This is a latitudinally-resolved MBL product derived from weekly measurements of the four trace gases

135   considered in this study. For time periods before the beginning of the NOAA MBL product we extend the time series based on different sources depending on the trace gas. For CO_2 before 1979 and N_2O before 2001, we use the CMIP6 reference time series from Meinshausen et al. (2017). For SF_6 before 1997, we use scaled Cape Grim mixing ratios based on Engel et al. (2008), which are very similar to the CMIP6 reference values. For CH_4 before 1983, we use annual average mixing ratios from Etheridge et al. (1998). For each trace gas we add on an average

140   seasonal cycle and latitudinal gradient based on the earliest available five years of the NOAA MBL product.

3 Method

145   The mixing ratio, χ, of a trace gas, i, at a location, $\boldsymbol{x}$, and time, t, can be expressed as:

$$\chi_i(\boldsymbol{x},t) = \int_0^\infty \chi_{io}(t-t')e^{-t'/\tau_i(\boldsymbol{x},t')}G(\boldsymbol{x},t,t')dt', \tag{1}$$

where G is the age spectrum, t' is the transit time from a source region to the location $\boldsymbol{x}$, $\chi_{io}(t-t')$ is the mixing ratio time series at the source region and τ_i is the path dependent lifetime of the trace gas (Fig. 1) (Schoeberl et al., 2000; Ehhalt et al., 2007). The age spectrum represents the distribution of transit times since an air parcel was last at the source region as shown schematically by the different colored lines in Figure 1. The age spectra are assumed to have an inverse Gaussian functional form given by

$$G(\boldsymbol{x},t,t') = \sqrt{\frac{\Gamma^2}{4\pi R t'^3}} \, exp\left(\frac{-\Gamma^2(t'-\Gamma)^2}{4Rt'}\right) \tag{2}$$

where the mean age is given by $\Gamma = \int_0^\infty t'G(\boldsymbol{x},t,t')dt'$, the width of the spectrum is given by $\Delta^2 = \frac{1}{2}\int_0^\infty (t'-\Gamma)^2 G(\boldsymbol{x},t,t')dt'$ and the ratio of moments $R = \Delta^2/\Gamma$ (Hall and Plumb, 1994; Waugh and Hall, 2002).
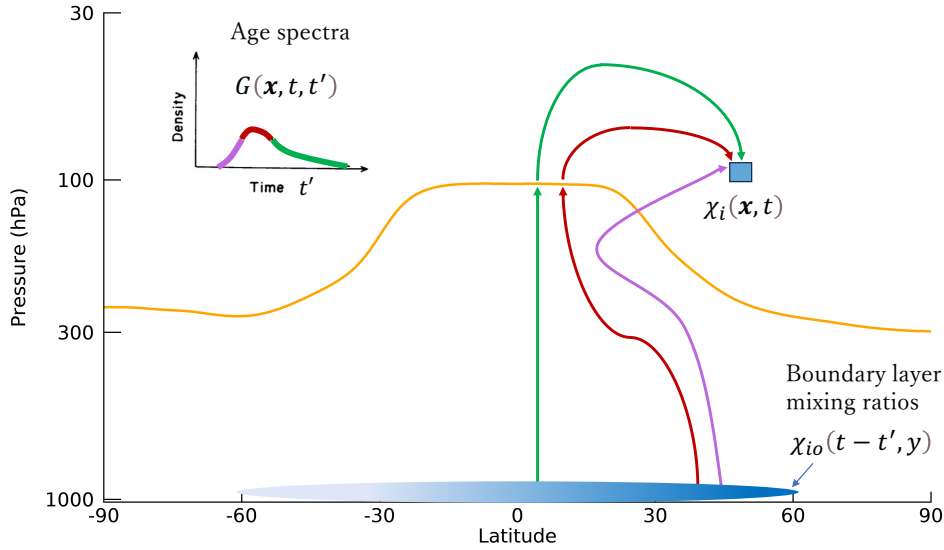
Figure 1. *Schematic of the age of air with the surface as the source region. Different pathways to the sampled region (**x**) are represented by the colored lines with different surface latitudinal origins (y) and time scales of transport (t') represented by the age spectra (G).*

The ratio of moments R, which is a measure of the width of the age spectra, is a largely unconstrained quantity and so we allow a range of values from 0.1-2.5 years for each possible Γ in the optimization calculation (Fig. S1). Most studies of age of air have used values of R ranging from 0.7-1.25 years based on model estimates (e.g., Hall and

Plumb, 1994; Volk et al., 1997; Engel et al., 2008). However, with a better understanding of the effect of the exponential tail of G for $t' > 10$ years, the model estimates of R have increased to values of 1.5 years or more with

170   considerable variability in the stratosphere (e.g., Diallo et al., 2012; Ploeger and Birner, 2016; Fritsch et al., 2020).

The source region for our calculation is the Earth's surface even though most previous stratospheric age of air studies have used the tropical tropopause since that is the primary entry region for air to the stratosphere above 380K (e.g., Andrews et al., 2001; Engel et al., 2009). There are a number of reasons we choose to use the surface as the

175   source region: (1) we have long-term measurements of all the trace gases at the surface which is not the case for the tropical tropopause, (2) we can obtain information about the surface source latitude regions with our optimization technique, (3) most modeled mean ages use the surface as the source region and (4) we can calculate ages in the troposphere and lowermost stratosphere with the same technique as the stratospheric overworld.

180   Following the techniques of Hauck et al. (2020) and Ray et al. (2022), we partition the age spectra into a part with a tropical (30°S-30°N average) surface source, g_{TR}, and a part with a latitudinally varying surface source, g_V. The partitioning of the age spectra in this way is primarily due to a recognition that the extratropical UTLS can be influenced by local convective transport from the extratropical surface (e.g. Herman et al., 2017; Ray et al., 2022). A surface source that is only represented by a tropical average, as in most previous age of air studies, will not

185   account for these extratropical surface influences that can be important for trace gases with large latitudinal gradients. The partitioned age spectra are expressed as

$$G(\Gamma, \Delta, t') = g_{TR}(\Gamma, \Delta, t') + g_V(\Gamma, \Delta, t'). \tag{3}$$

190   The lowercase g is used to indicate age spectra that are non-normalized, in contrast to the uppercase G total age spectra that are normalized. The age spectra g_V do not vary with latitude but are convolved with surface mixing ratio time series from varying latitudes as part of the optimization as will be shown in the next section, whereas the age spectra g_{TR} are always convolved with the tropical average surface mixing ratios. Note that we have now expressed the age spectra as a function of Γ and Δ since those are the parameters in G we allow to vary in the

195   convolutions with the χ_{io} time series. The partitioned age spectra are expressed as fractions, f, of the G as a function of t'.

$$g_{TR}(\Gamma, \Delta, t') = f(t')G(\Gamma, \Delta, t') \tag{4}$$

200    $$g_V(\Gamma, \Delta, t') = \big(1 - f(t')\big)G(\Gamma, \Delta, t') \tag{5}$$

The fraction f has an age dependence with $f(t' < t'_i) = 0$, $f(t' > t'_f) = 1$ and an exponential form between t'_i and t'_f, which are the transition ages between the latitudinally varying and purely tropical surface source regions. Based on Ray et al. (2022) where a value of $t'_f \approx 150$ days was found to be optimal above 380K, we use values of $t'_i =$

205   0.4 years and $t_f' = 0.6$ years (Fig. S2). The Ray et al. (2022) study showed the importance of the extratropical

surface as a source region for certain locations and seasons in the lower stratosphere, such as over North America

during the monsoon season. But for other locations and seasons the tropical surface may be the most important

source region for the youngest ages in the stratosphere and the calculation allows for that possibility.

210   *3.1 Convolutions*

Convolutions of the age spectra with the surface mixing ratio time series for each trace gas are performed for the

time period of available *in situ* measurements. The convolved mixing ratios, χ_i, are given by

215
$$\chi_i(\Gamma, \Delta, y_o, t) = \chi_{iTR}(\Gamma, \Delta, t) + \chi_{iV}(\Gamma, \Delta, y_o, t) \tag{6}$$

where the subscript o refers to a surface quantity, y_o is a surface source latitude parameter and

$$\chi_{iTR}(\Gamma, \Delta, t) = \int_0^\infty \chi_{ioTR}(t - t', y_{oTR}) g_{TR}(\Gamma, \Delta, t') dt' \tag{7}$$
220

$$\chi_{iV}(\Gamma, \Delta, y_o, t) = \int_0^\infty \chi_{ioV}(t - t', y_o) g_V(\Gamma, \Delta, t') dt' \tag{8}$$

The surface mixing ratio time series χ_{ioTR} are tropical averages from 30°S-30°N (y_{oTR}) in the case of χ_{iTR}, or

latitudinally varying averages in 10° intervals ranging from 60°S-60°N (y_o) in the case of χ_{iV}. Note that there is no

225   latitudinal dependence for χ_{iTR} since y_{oTR} represents a single tropical average latitude region.

Examples of χ_{SF6} and χ_{CO2} as a function of Γ for early November 1994 are shown in Fig. 2. The dependence of χ_i

on y_o and R are shown separately to reveal the Γ range most sensitive to these parameters. χ_i varies most strongly

with y_o for $\Gamma < 2$ years (Fig. 2a,b). This is expected due to the functional form of g_V which peaks for $t' < 0.5$

230   years. Even for $\Gamma = 2$ years, g_V is a significant portion of the total age spectrum G (Fig. S2). But for $\Gamma > 2$ years

the contribution of g_V to G decreases rapidly and thus the dependence on y_o as well. The values of t_i' and t_f' are of

course not known precisely and likely vary with time and location as shown for a limited time and region in Ray et

al. (2022). Changes in the assumed time scales of transport from y_o will change the χ_i distributions in Fig. 2

somewhat but we do not expect moderate time scale changes to change our results. One reason for this is the

235   frequent opposite dependence of the two trace gas convolutions on y_o so that even if the χ_i distributions were

broadened based on different assumed transport time scales, the optimal solutions will be confined to the relatively

narrow overlap region of the distributions. We do not explore the effects of the values of t_i' and t_f' any further in this

work but it is an interesting aspect that would be helpful to understand better.

240   The surface latitudinal gradient of χ_{CO2} is known to have substantial seasonal variability with larger values of χ_{CO2} in the NH during boreal winter and a reversed latitudinal gradient in boreal summer (https://gml.noaa.gov/ccgg/mbl/), whereas the latitudinal gradient of χ_{SF6} has essentially no seasonal variability with larger values in the NH. For NH Fall, the contrast between the χ_{SF6} and χ_{CO2} dependence on y_{ov} for $\Gamma < 2$ years is stark, with larger values of χ_{SF6} for more northern values of y_{ov} and the opposite for χ_{CO2}. This is due to the

245   opposite latitudinal surface gradients of these trace gases in the preceding NH summer, shown by the minimum of χ_{CO2} for the most northern values of y_o at $\Gamma = 0.3$ years. The reversed latitudinal dependence of χ_{SF6} and χ_{CO2} persists to $\Gamma \approx 2$ years since g_V remains influenced by the NH summer for all values of Γ. Values of χ_{CO2} for April have the opposite latitudinal dependence (Fig. S3) as in November due to the opposite latitudinal surface gradient of CO_2 in NH winter compared to summer. For $\Gamma > 3$ years, the values of χ_i have negligible dependence on y_{ov} and

250   correspond to those using only χ_{ioTR} (dashed green lines in Fig. 2). Thus, for older mean ages the values of χ_i are similar to previous studies that used the average of Mauna Loa and Samoa station data (e.g., Andrews et al., 2001).
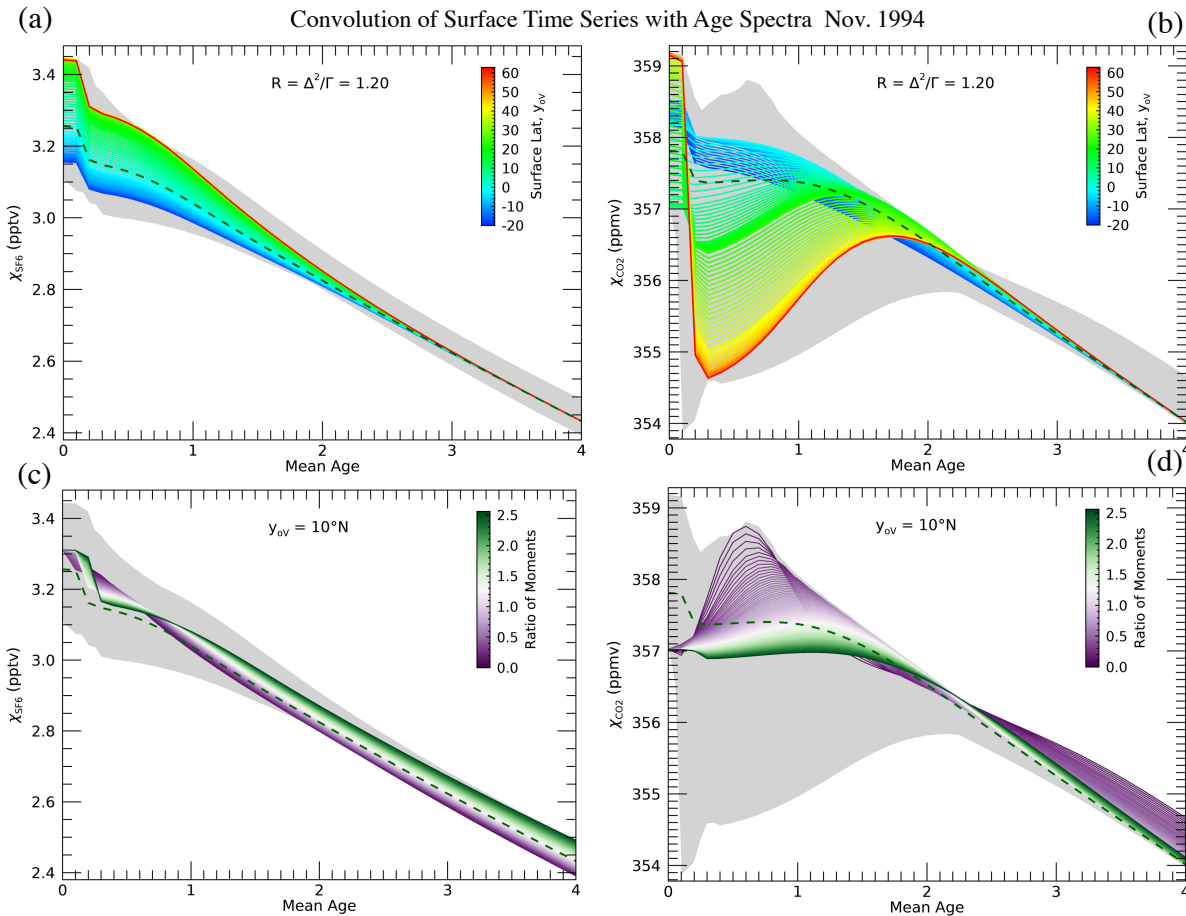
Figure 2. Convolutions of SF_6 (a,c) and CO_2 (b,d) surface mixing ratios with a range of age spectra and mean ages.

255   *These convolutions could be compared to stratospheric measurements of each trace gas in early November 1994 (NH Fall). The dependence of the convolutions on surface source latitude is shown in the top row while the*

260

The dependence of χ_{SF6} and χ_{CO2} on R for $y_o = 10°N$ contains a significant spread for nearly all values of Γ but especially for $\Gamma > 2$ years, in contrast to the dependence on y_o (Fig. 2c,d). In NH Fall, χ_{SF6} and χ_{CO2} have the opposite dependence on R for $\Gamma > 1$ year, while for NH Spring the dependence is the same for both trace gases (Fig.

265   S3c,d). This again reflects the seasonal change of the CO_2 surface gradient and how the shape of the age spectra can make the convolutions sensitive to a particular season.

A noticeable feature of the NH Fall convolutions is the wide range of possible values of χ_i for the same Γ, especially χ_{CO2} for $\Gamma < 2$ years as shown by the grey shading (Fig. 2). The implication of this is that unless there is high

270   confidence in y_o and R for a particular airmass, the uncertainty in Γ from either SF₆ or CO₂ alone can be significant. But in combination, the intersection of χ_{SF6} and χ_{CO2} can provide a much narrower range of possible Γ, which we show below to not only reduce the uncertainty in Γ compared to using a single trace gas but also reveals optimal values of y_o and R.

275   *3.2 Adjustments for photochemistry*

Before two trace gases can be used in an optimization of age of air, their photochemical lifetimes (Eq. 1) and thus potential adjustments to the measured mixing ratios (χ_i^*), must be considered. A reduction of χ_{CO2}^* has traditionally been made before Γ is calculated due to the conversion of CH₄ to CO₂ in the atmosphere (e.g., Boering et al., 1996;

280   Daniel et al., 1996). This adjustment requires simultaneous measurements of CH₄ or N₂O along with CO₂ and has assumed that the difference between the surface average CH₄ at the time of the measurement and the CH₄ measured in the stratosphere is entirely due to the oxidation of CH₄ to CO₂. In the case where a simultaneous χ_{CH4}^* was not available and χ_{N2O}^* was, then a CH₄-N₂O relationship has been used to approximate χ_{CH4}^* (e.g., Andrews et al., 2001).

285

While the adjustment of χ_{CO2}^* due to CH₄ oxidation is typically small since CH₄ surface mole fractions have been ~1.7-1.9 ppm over the past few decades, the effect on Γ estimates can be significant based on the nonlinear shape of the χ_{CO2} distributions shown in Figs. 2b and 2d. Furthermore, it has been shown in modeling studies that not all of the oxidized CH₄ is converted into CO₂ (Boucher et al, 2009; Shindell et al., 2017). Although the average

290   conversion percentage in these two studies was 61% and 88%, essentially all of the conversion in the stratosphere ends up as CO₂. Based on these results we use a 95% average conversion of CH₄ into CO₂ and we also increase the uncertainty on χ_{CO2}^* by 5% of the CH₄ loss to account for some uncertainty in the conversion percentage.

Another aspect of the CO_2 adjustment due to CH_4 oxidation that we reevaluate is the use of the surface average CH_4 mixing ratio at the time of measurement to subtract from χ^*_{CH4}. The mixing ratios that should be used are the convolution values χ_{CH4} since these represent the actual boundary conditions of CH_4. The values of χ_{CH4} have a larger dependence on y_{oV} (Fig.S4) than either the Γ or R. The difference between the surface average CH_4 at the time of stratospheric measurement used in previous studies, and values of χ_{CH4} is typically 0.02-0.03 ppm but can be greater than 0.05 ppm for $\Gamma < 1$ year. On its own, this difference and the subsequent change in the adjustment of χ^*_{CO2} is small, but as mentioned earlier can have a nonlinear effect on the age calculation. The use of χ_{CH4} is also simply the correct technique to estimate the entry or initial CH_4 mixing ratios for any measurement location, and especially in an optimization with multiple tracers.

For SF_6 it has been known for some time that mesospheric loss has an impact on age of air calculations with this trace gas (Hall and Waugh, 1998; Hall et al., 1999; Andrews et al., 2001). The old age bias in Γ from SF_6 was thought to be largely confined to airmasses in or near the winter polar vortex (e.g., Ray et al., 2017) and not in the mid-latitudes (Engel et al., 2009; Ray et al., 2014). Based on recent studies we now understand that the old age bias in Γ from SF_6 has a latitudinal and temporal dependence on the mixing ratio of SF_6 and that a Γ bias correction can be found and applied (Loeffel et al., 2022; Garny et al., 2024). This is an important advancement in the use of SF_6 as an age of air tracer and without it an optimization of the kind described here would not be possible.

We make SF_6 adjustments based on a correction technique from the work of Garny et al. (2024) that parameterizes the expected Γ bias as a function of Γ and time. We convert this Γ bias into a mixing ratio adjustment via the SF_6 tropospheric growth rate over the previous year and add this estimated mesospheric loss to χ^*_{SF6}. There are uncertainties inherent to this technique, primarily due to the relatively new Γ bias estimates that are based on a single model thus far. We do not explicitly add an additional uncertainty to the adjusted values of χ^*_{SF6} (denoted as χ^*_{aSF6}), but we do investigate possible uncertainties in the adjustments through a scaling method that is described below.

3.3 Optimization

We now look at an example of a specific measurement time and place to demonstrate the optimization technique. The example is from an ER-2 flight in early November 1994 during the ASHOE-MAESA campaign at a time when simultaneous χ^*_{SF6} and χ^*_{CO2} were available. The range of χ_{CO2} and χ_{SF6} values are the same as shown by the grey shading in Fig. 2 since those values are relevant for the November 1994 time period. The photochemically adjusted χ^*_i values, denoted as $\chi^*_{ai}(\Gamma)$, have a dependence on Γ since as described above, for SF_6 the older the Γ is the more loss will have occurred. Likewise for CO_2 the χ_{CH4} values are dependent on Γ. The difference between the χ^*_i and $\chi^*_{ai}(\Gamma)$ values for both trace gases are shown in Figs. S5 and 3. The uncertainty on $\chi^*_{ai}(\Gamma)$ is indicated by χ^*_{eai} but

for the two species used here only CO_2 has a change in the size of the uncertainty from the original measurement

330   due to the uncertainty in CH_4 production.

A range of possible mean ages, surface source latitudes and ratios of moments (Γ, y_o and R) can be found for each trace gas based on agreement of the convolutions (χ_i) with the adjusted measured mole fractions ($\chi_{ai}^*(\Gamma)$) within the uncertainty range ($\pm\chi_{eai}^*$). For the example shown here, the values of Γ compatible with $\chi_{aCO2}^*(\Gamma)$ range from 0.1-

335   2.6 years, while for SF_6 the Γ range is 2.4-2.9 years (Figs. S5 and S6). Figure 3 zooms in on the range of Γ and χ_i around where both trace gases have similar Γ solutions. The χ_{SF6} values that agree with $\chi_{aSF6}^*(\Gamma)$ within $\pm\chi_{eSF6}^*$ are shown by the magenta symbols and labeled $\chi_{SF_6}(\Gamma_{SF6})$ in Fig. 3a and likewise for CO_2 in the orange symbols and labeled $\chi_{CO_2}(\Gamma_{CO2})$ in Fig. 3b. The Γ resolution of our calculation was 0.05 years which is why there are distinct columns of symbols in the figure.

340

Since any optimal solutions must be compatible with both trace gases, we need to look at how the possible Γ, Δ, y combinations from one tracer affect the χ_i values of the other tracer. The values of χ_{SF_6} with CO_2 solutions are shown by the orange symbols in Fig. 3a and labeled $\chi_{SF_6}(\Gamma_{CO2})$ and likewise the values of χ_{CO_2} with SF_6 solutions are shown by the magenta symbols in Fig. 3b and labeled $\chi_{CO_2}(\Gamma_{SF6})$. Most of the $\chi_{SF_6}(\Gamma_{CO2})$ values are greater than

345   the χ_{aSF6}^* values within $\pm\chi_{eSF6}^*$, while most of the $\chi_{CO_2}(\Gamma_{SF6})$ values are less than the $\chi_{aCO2}^*(\Gamma)$ values within $\pm\chi_{eaCO2}^*(\Gamma)$. However, there is a region of overlapping solutions for both trace gases as indicated by the green symbols and labeled $\chi_{SF_6}(\Gamma_\cap)$ and $\chi_{CO2}(\Gamma_\cap)$ where $\Gamma_\cap$ represents the intersection of possible Γ, Δ, y combinations.
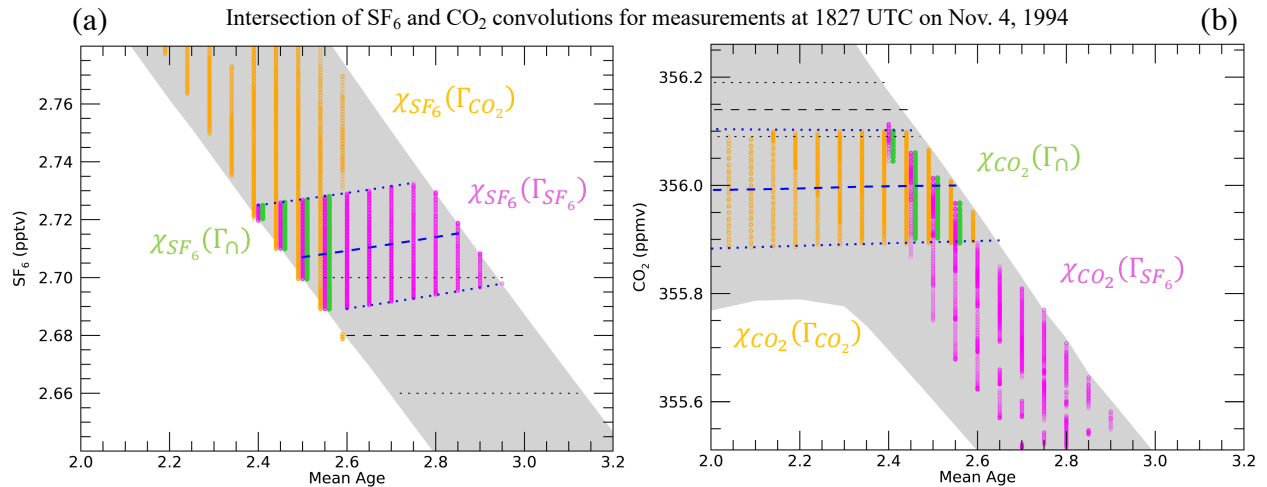
350   Figure 3. *Zoomed in convolutions similar to Fig. 2 but also including the simultaneous measured SF_6 and CO_2 mixing ratios from the ASHOE-MAESA ER-2 flight on Nov. 4, 1994 at 1827 UTC in the black dashed lines with uncertainties indicated by the dotted black lines. The adjusted mixing ratios and uncertainties are indicated by the dashed and dotted blue lines. The range of solutions for SF_6 alone ($\chi_{SF_6}(\Gamma_{SF6})$) are indicated by the magenta symbols in (a) and likewise for CO_2 alone ($\chi_{CO_2}(\Gamma_{CO2})$)by the orange symbols in (b). The values of χ_{SF_6} with the*

355 *CO_2 solutions ($\chi_{SF_6}(\Gamma_{CO2})$) are shown by the orange symbols in (a) and likewise the values of χ_{CO_2} with the SF$_6$*

solutions ($\chi_{CO_2}(\Gamma_{SF6})$) are shown by the magenta symbols in (b). The intersection of solutions that agree with both

trace gases within uncertainties are indicated by the green symbols and labeled $\chi_{SF6}(\Gamma_\cap)$ and $\chi_{CO2}(\Gamma_\cap)$. Dashed

lines are as described in the caption of Figure S5.

360 The intersection of solutions is the basis of the optimization used to find a single best solution for each set of

measurements. We first find normalized differences expressed as $\delta\chi_i = |\chi_i - \chi_{ai}^*|/\chi_{eai}^*$ (Fig. S6). A combined

difference quantity, $\delta\chi_\cap$, for the intersection of solutions is defined as the average of the $\delta\chi_i$ values (Fig. S7),

$$\delta\chi_\cap = (\delta\chi_{CO_2}(\Gamma_\cap) + \delta\chi_{SF6}(\Gamma_\cap))/2. \tag{9}$$

365

From $\delta\chi_\cap$ we define weighting functions $W_\cap = (\max(\delta\chi_\cap) - \delta\chi_\cap)/\sum \delta\chi_\cap$ to be multiplied by the set of transport

parameters within the intersection of solutions to find the optimum values

$$\Gamma_o = W_\cap\Gamma_\cap, \quad \Delta_o = W_\cap\Delta_\cap, \quad y_o = W_\cap y_\cap. \tag{10}$$

370

Thus, for each measurement location there is a single set of transport parameters Γ_o, Δ_o, y_o that are optimized for χ_{ai}^*

of both trace gases (Fig. S8).

Note that the optimization can be performed for a single trace gas by following the same general procedure

375 described above. The range of possible transport parameters is larger for a single trace gas compared to an

optimization with two or more trace gases and so the uncertainty on the results will be larger, and there will be a

higher probability that the optimized transport parameters are 'incorrect'. In the example measurement location

used here, if the optimization were performed only on CO_2, Γ_o would be much younger than the result with both SF$_6$

and CO_2.

380

3.4 Offsets to measured mixing ratios

In some cases, the intersection of possible solutions for SF$_6$ and CO_2 within uncertainties is small or there is no

intersection at all. This lack of overlap could be due to various reasons, such as an inconsistent calibration between

surface and atmospheric measurements or an inaccurate correction for photochemical loss or production of a trace

385 gas. Since there can be only one set of transport parameters in the real atmosphere at any one time and place, a lack

of an intersection of solutions implies then an offset in one or both trace gases at the measurement location is

necessary to perform the optimization.

390 To account for the possibility that an offset of either trace gas is needed to obtain a solution set, we ran an ensemble

of optimizations (see Supplement) that swept over a grid of mixing ratios with positive and negative offsets from the

measured value of each trace gas for each measurement location. Note that we offset the adjusted (χ_{ai}^*) mixing ratios and use the same uncertainties (χ_{eai}^*). The optimization performed for each member of the offset ensemble produces a unique set of transport parameters $\Gamma_o(s), \Delta_o(s), y_o(s)$ and a minimum value of the combined normalized

395   difference $\delta\chi_{\cap min}(s)$, with the dependence on s added to denote the offset ensemble member (Fig. S9).

There are a number of possible ways to select the best member of the ensemble and thus the best overall set of solutions. We chose to use an optimization method that is consistent with that used for each member of the ensemble as described above and the details are included in the supplement. Most of the offset values are small,

400   especially for CO_2, but there are certain measurement times and locations where the optimal offset of SF_6 is significant. Figs. 4 and 5 show SF_6 and CO_2 average optimal offset values as a function of normalized N_2O for the 1990s and 2020s data. Normalized N_2O (χ_{N2On}) is defined as $\chi_{N2O}^*(t)/\overline{\chi_{N2Oo}}(t)$, that is, the measured atmospheric N_2O mixing ratio divided by the global mean surface N_2O mixing ratio at the time of measurement. N_2O has often been used as a quasi-vertical coordinate when displaying *in situ* data due to the compact relationships of long-lived

405   trace gases and Γ with N_2O (e.g. Plumb and Ko, 1992; Andrews et al., 2001). We use normalized N_2O in this figure and others in order to account for the growth rate of N_2O over time, enabling the comparison of compact relationships with N_2O over years or decades.

410
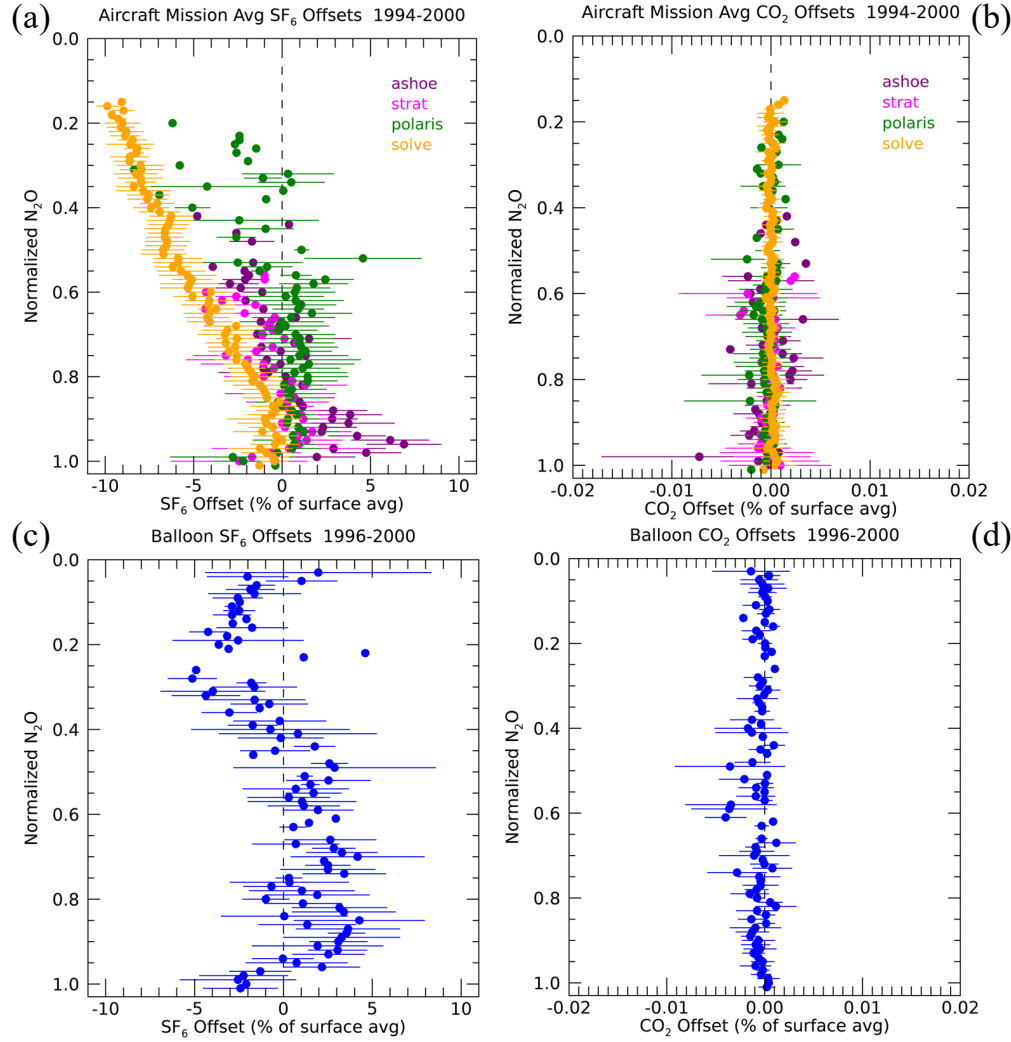
Figure 4. *Offset values (χ_{is}) divided by the global average surface mixing ratios of each trace gas at the time of measurement and binned by normalized N₂O (χ_{N2On}) for SF₆ (a,c) and CO₂ (b,d). The top row (a,b) shows normalized offset values binned separately for four different aircraft missions in the 1990s and the bottom row (c,d) shows normalized offset values averaged over seven OMS balloon flights in the 1990s. Essentially all of the data*

415 *represented in this figure are from the stratosphere at altitudes up to ~32 km.*

The offset values are also normalized by the global average surface mixing ratios of each trace gas and displayed as a percentage. There are several features of note in Figs. 4 and 5. The first is that χ_{CO2s} (where the subscript *s* refers to an offset value) is essentially zero, <0.01% compared to an annual growth rate of 0.3-0.5%, for all values of N₂O

420 for both the 1990s and 2020s data. This follows from the symmetric nature of the offset ensemble results in CO₂ as shown by the example in Fig. S9. This implies that there is no advantage in the optimization calculation to offset CO₂ either positively or negatively in order to better agree with any set of SF₆ solutions. Further implications are

that the calibration between CO_2 measured *in situ* in the atmosphere and the surface have remained consistent over several decades and that the photochemical adjustment of CO_2 does not appear to have a significant bias.

425
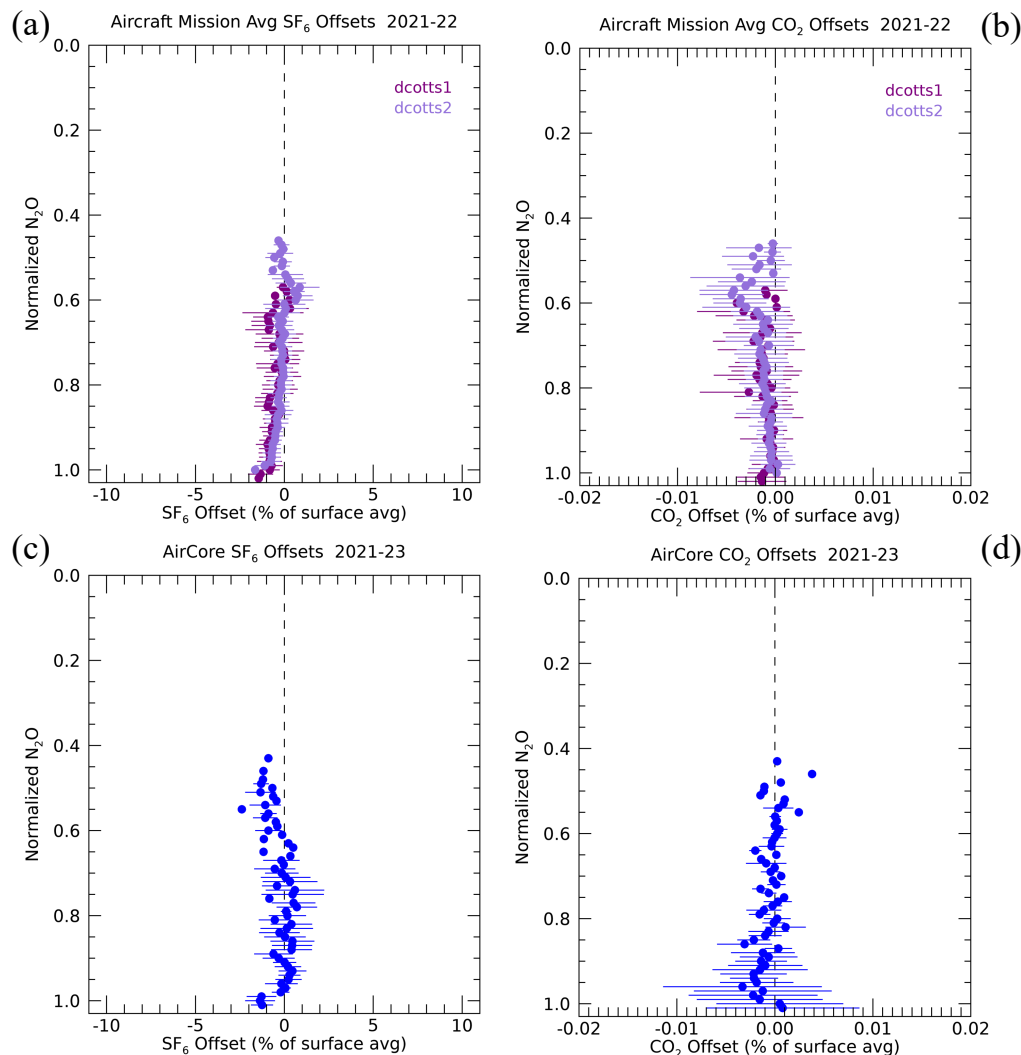
Figure 5. *Same as Fig. 4 but for two DCOTSS aircraft missions in the 2020s (a,b) and for routine AirCore balloon flights in the 2020s (c,d).*

430   A second feature of note is the size of χ_{SF6s} for the 1990s data compared to that from the 2020s. In the 1990s, χ_{SF6s} ranges from -9% to +7% at a time when the annual growth rate of SF_6 was ~5%/year, while in the 2020s χ_{SF6s} ranges from -2% to +1% at a time when the annual growth rate was ~3.5%/year. Thus, the χ_{SF6s} values translate to Γ shifts from -1.8 to +1.4 years in the 1990s and -0.5 to +0.3 years in the 2020s. As mentioned earlier, these χ_{SF6s} values could be due to an inaccurate SF_6 photochemical loss adjustment that we apply in the optimization based on

435   the Garny et al. (2024) study. If the photochemical loss was estimated to be larger than reality, χ_{aSF6}^{*} would be too large and the optimization would compensate by producing negative χ_{SF6s} values to agree with CO_2 and vice versa. The fact that there is essentially an equal amount of positive and negative χ_{SF6s} values, outside of the SOLVE

mission that we will discuss below, and that the 2020s χ_{SF6s} values are mostly near zero suggest that there is not a systematic error in the photochemical loss adjustments. There can be certain locations and times when the

440 adjustment could be too large or small but this is likely due to known limitations of the simplified adjustment used here, such as in the region of the polar vortex where the gradients of SF_6 loss are large.

A third feature, notable in Fig. 4, is the nearly linear dependence and large negative values of χ_{SF6s} as a function of N_2O during the SOLVE mission. These large negative values could be due to either assumed photochemical loss

445 that is much too large or a calibration issue with χ^*_{SF6} during the mission. Based on the outlier nature of χ_{SF6s} during SOLVE compared to other missions as well as the size of the photochemical loss error that would be necessary to cause these values (>100% for χ_{N2On}>0.3) it is unlikely the assumed photochemical loss is the primary cause. There was a known SF_6 calibration scale change during SOLVE (https://espoarchive.nasa.gov/archive/browse/oms/Balloon) that resulted in the value of the Volk et al. (1997) delay

450 term from the surface to the tropical tropopause ($\delta\Gamma$) to be changed from +0.8 years used in previous missions to -0.8 years in SOLVE. A negative value of $\delta\Gamma$ is obviously non-physical but was necessary to calculate reasonable Γ values due to the relatively large χ^*_{SF6} compared to the surface values. This change in the value of $\delta\Gamma$, even considering the different source region of the surface compared to the tropical tropopause, is enough to explain most of the negative χ_{SF6s} values from the optimization. Thus, this analysis clearly points out a significant high bias in

455 χ^*_{SF6}, especially at the highest altitudes and latitudes (lowest χ_{N2On}), measured on the ER-2 during the SOLVE mission.

3.5 Single Trace Gas Optimizations

460 In order to utilize the large number of *in situ* measurements with no simultaneous or near-simultaneous measurements of a second age of air trace gas, we also perform the optimization described here on a single trace gas. A single trace gas optimization is not ideal but we make use of the relatively tight $\Gamma - \chi_{N2On}$ and $R - \chi_{N2On}$ correlations derived from the two trace gas optimizations to constrain those parameters for a single trace gas optimization (Figs. S10 and 6). Based on the measured χ_{N2On} at any location we choose a range of possible Γ and R

465 consistent with the correlations based on other missions during a similar time period and perform the optimization only within the limited range of each parameter. Thus, our technique requires a near-simultaneous measurement of N_2O with any single age of air trace gas.

The lack of simultaneous measurements can be due to a mismatch in instrument sampling rates, as is the case for

470 CO_2 and SF_6 mentioned in Sect. 2, or the lack of measurements of two different age of air trace gases on a particular airborne platform or mission. The single trace gas optimization is often most desirable with CO_2 since there are usually nearly two orders of magnitude more measurements available during a mission compared to SF_6. Since χ_{CO2s} is negligible for all of the measurements considered in this study, we can reasonably perform the optimization with CO_2 alone without scaling. In the 2020s, χ_{SF6s} is also minimal so we can perform the single trace gas

475   optimization with SF_6, for instance, with data from the SABRE mission in 2023 when CO_2 measurements were not
available.

4 Results

480   *4.1 1990s*

The 1990s was the last time period of extensive *in situ* measurements from both aircraft and balloon platforms of
long-lived trace gases and Γ calculated from CO_2 and SF_6 (denoted Γ_{CO2} and Γ_{SF6}) in the stratosphere at altitudes
above 16 km. The Γ_{CO2} and Γ_{SF6} values from this time period have been used extensively over the past several
485   decades to compare to model output, especially the use of the 'wing plot' of Γ in the 20km altitude region as a
function of latitude (Figure 6) (Waugh et al., 1997; Hall et al., 1999; Andrews et al., 2001; Waugh and Hall, 2002;
Strahan et al., 2011; Diallo et al., 2012; Chabrillat et al., 2018; Dietmuller et al., 2018; Ploeger et al., 2019). The
general features of Figure 6 are similar to versions of this plot shown in previous publications. The seasonally
resolved averages reveal that the spread of the mean ages in most latitude bins is driven by expected seasonal
490   variability, most noticeable in the NH subtropics and polar regions, rather than an uncertainty on the measurements
or mean age estimates. The latitudinal averages in Figure 6 also have missing values and some outlier points, both
of which are expected from aircraft sampling even during this peak stratospheric sampling period.
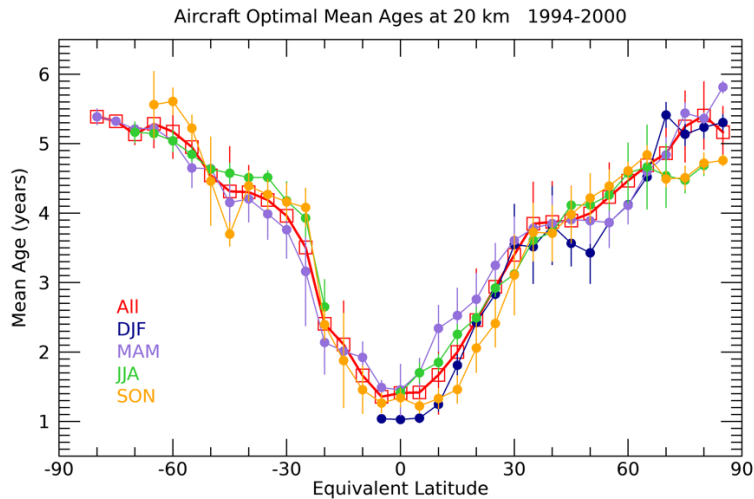
495   Figure 6. *Mean age at 20 km altitude as a function of latitude for aircraft measurements from the 1990s, commonly*
referred to as the 'wing plot'. The averages for different seasons as well as for all times at each latitude are shown
separately.

The compact $\Gamma - \chi_{N2On}$ relationship has also been commonly used as a transport metric and method to compare *in*
500   *situ* data and model output (e.g. Hall et al., 1999; Andrews et al., 2001; Strahan et al., 2011; Birner et al., 2020). As

mentioned in Sect. 3.5, we utilize the $\Gamma_o - \chi_{N2On}$ relationship in our optimizations for cases with a single trace gas measurement and we also can compare the relationships found here with those from previous Γ techniques.
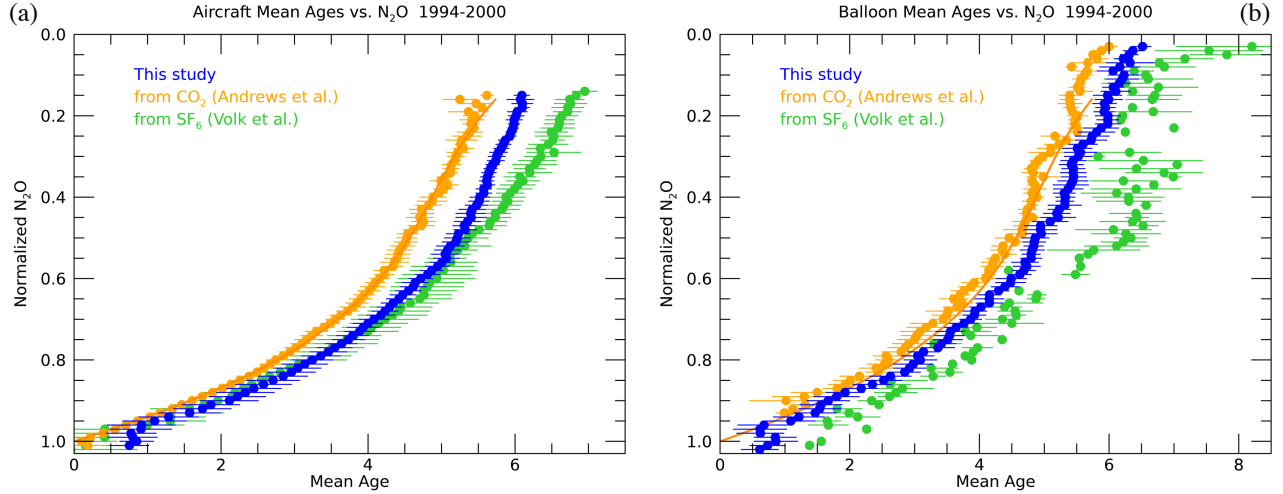
505   Figure 7. *Mean age vs. normalized N2O for aircraft (a) and balloon (b) measurements from the 1990s. The results from this study are shown in blue, those based on previously published CO2 in orange and from SF6 in green. The aircraft measurements are from the four ER-2 missions shown in Fig. 4a. The uncertainties represent the standard deviation of the mean ages within each N2O bin. The functional form from Andrews et al. (2001) translated to normalized N2O is shown as the solid orange line in both plots.*

510

Figure 7 shows $\Gamma - \chi_{N2On}$ correlations for all of the 1990s aircraft and balloon data. Each set of correlations comes from essentially the same sampled latitudes, altitudes and seasons for each measurement platform. The correlations include measurements from the tropics to polar latitudes and nearly all seasons for the aircraft data demonstrating the remarkable compactness of the correlations. The Γ_{SF6} bias of up to two years due to SF6 photochemical loss at

515   that time is seen by comparing the Γ_{SF6} and Γ_{CO2}. Values of Γ_o typically fall between the values of Γ_{SF6} and Γ_{CO2}. We clearly expect Γ_o to be younger than most of the Γ_{SF6} values since we account for photochemical loss, while we also expect Γ_o to be older than Γ_{CO2} by at least three months since the source region of our calculation is the surface compared to the tropical tropopause for the previous calculation. To compare more directly to previous mean age estimates we could, for instance, subtract three months from Γ_o but the point of Figure 7 is to show that the mean

520   ages calculated in this study are different from previous estimates and that is to be expected for the reasons discussed above.

The aircraft Γ_{CO2} from the 1990s are based on χ_{N2O}^* rather than χ_{aCO2}^* for values of $\chi_{N2On} > \sim 0.8$ (Andrews et al., 2001), which explains the tight relationship and no variability in Γ_{CO2} in this range in Fig. 7a. This relationship was

525   based on measurements in the tropical tropopause region during this time. While this $\Gamma_{CO2} - \chi_{N2On}$ relationship was valid for the particular time and place of the original measurements, a fixed relationship of this sort does not allow

detection of changes in the relationship over time or allow for variation in latitude. The Γ_o values in this study are derived independently of any $\Gamma - \chi_{N2On}$ relationship and yet produce very compact curves for both the aircraft and balloon data as seen in Fig. 7. There is at least an order of magnitude more aircraft measurements compared to

530   balloon measurements resulting in the relatively more compact relationships in Fig. 7a compared to those in Fig. 7b.
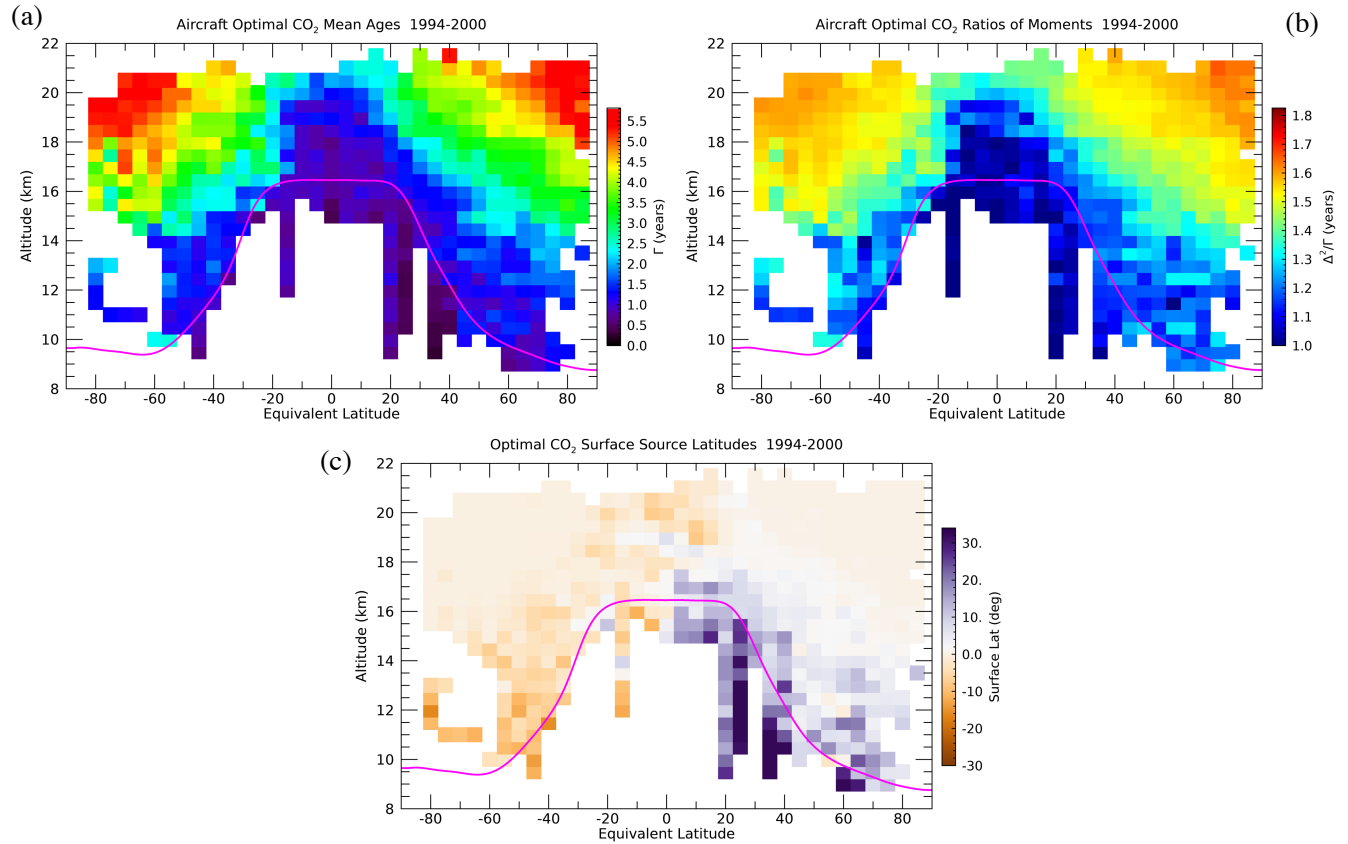
Figure 8. *Equivalent latitude vs. altitude distributions of mean ages (a), age spectra ratios of moments (b) and*

535   *surface source latitudes (c) from the CO₂ optimizations averaged over the 1990s aircraft missions. The grid spacing is 0.5 km in altitude and 5 degrees in latitude.*

Average distributions of the transport parameters derived from the optimizations with the 1990s aircraft measurements are shown in Figs. 8 and S11. The two figures reveal the difference in spatial coverage of where there

540   were near simultaneous measurements of SF_6 and CO_2 (Fig. S11) compared to CO_2 alone (Fig. 8). We focus here on the CO_2 optimizations shown in Fig. 8 since the more extensive number of measurements and spatial coverage gives a nearly complete picture of the average transport features in the upper troposphere and lower stratosphere.

One of the most notable features of the distributions in Fig. 8 is that they cover a range of latitudes and altitudes

545   including the troposphere, lowermost stratosphere and stratospheric overworld nearly from pole to pole. There have

been no previous Γ estimates from *in situ* measurements that span this spatial range. This is partly due to the original concept of age of air as a time scale since an air parcel crossed the tropical tropopause into the stratospheric overworld (Kida, 1983). Thus, many previous Γ estimates from *in situ* data have focused only on the stratospheric overworld with the tropical tropopause as the entry region (e.g. Boering et al., 1996; Volk et al, 1997; Andrews et al.,

550   2001; Engel et al., 2008). Subsequent studies have focused on the lowermost stratosphere with a modified age of air concept to account for multiple tropopause entry regions (e.g. Boenisch et al., 2009; Hauck et al., 2019, 2020). And interhemispheric tropospheric age of air from the NH surface to the SH surface has also been estimated from *in situ* surface measurements (Waugh et al., 2013; Holzer and Waugh, 2015). The Ray et al. (2022) study calculated Γ from the troposphere through the stratospheric overworld but just from one aircraft mission in the NH midlatitudes.

555

In general, the Γ_o distributions look as expected with the youngest ages in the troposphere, near the tropopause as well as in the tropical stratosphere, and the oldest ages at the highest latitudes and altitudes. Values of Γ_o at the tropopause vary with latitude, from ~0.5 years in the tropics to 1-1.5 years in the extratropics. The extensive *in situ* measurements of key long-lived trace gases in the 1990s provides a nearly complete view of the Γ_o distributions at

560   that time.

The distribution of R_o shown in Fig. 8b is a unique contribution of this study. The R_o distribution mirrors that of Γ_o with the smallest values near one year in the troposphere and tropical stratosphere, increasing to values >1.5 years at high latitudes and altitudes. The only other previously published distributions of R come from model output. Hall

565   and Plumb (1994) found values from 0.4-0.7 years throughout the stratosphere from global climate model output at that time. Based on this study, Engel et al. (2008) used a value of $R = 0.7\pm0.5$ years in their analysis of Γ trends from balloon measurements of CO_2 and SF_6. In contrast, Volk et al. (1997) used a value of $R = 1.25\pm0.5$ years to calculate mean ages from SF_6 measurements based on the model output from Waugh et al. (1997). Thus, the value of R has varied widely among models and has essentially been unconstrained by observations. More recent

570   modeling studies have revealed the sensitivity of R to the long age tail of G (e.g. Ploeger and Birner, 2016) and have found values of R up to 1.7 years in the extratropical lower stratosphere with appropriate extension of the age spectra tail (Fritsch et al., 2020). The magnitude and distribution of the R values shown in Fig. 8b compare well to those in Fritsch et al. (2020, Fig. 6b) and provide some of the first extensive validation of modeled values of R throughout the lower stratosphere.

575

The surface source latitude distribution range in Fig. 8c is also a unique result with Ray et al. (2022) the only known previous study to have calculated this quantity from trace gas observations, but over a more limited time and location. The latitudes shown in the figure are averages of y_o scaled by $\sum g_V$, which could be considered an extratropical fraction of air. We scale y_o this way to show where the extratropical surface source latitudes matter in

580   the optimization, which is primarily for locations where $\Gamma < {\sim}3$ years. For Γ older than this the extratropical surface contribution to the optimization is negligible and the source latitude is the equator. The most notable feature in the source latitude distribution is the hemispheric symmetry with surface latitudes from the same hemisphere as

the location of χ_i^* except for in the tropical stratosphere. There will of course be seasonal variability in this quantity which we will not describe further here. This quantity could also be used to compare to surface source region attributions in the stratosphere from model output (e.g. Yan et al., 2021).
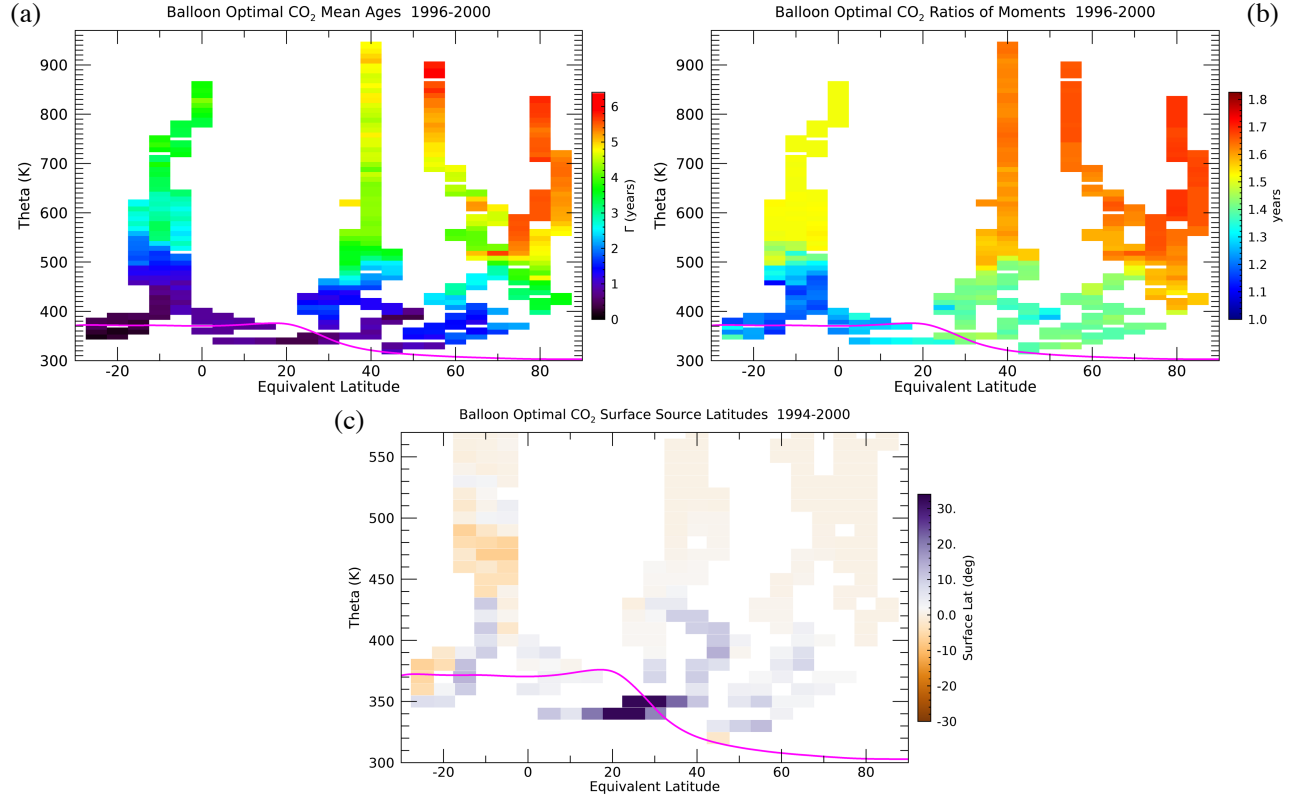
Figure 9. *Similar to Fig. 7 but for OMS balloon CO_2 optimizations averaged over the 1990s and the vertical coordinate is potential temperature. Note that the mean age range in (a) and the latitude scale have been changed from Fig. 8 to better match the balloon sampling and the theta scale is cut off for the surface source latitudes. Grid spacing is 10 K in potential temperature and 5 degrees in latitude.*

Distributions of the three transport quantities from the optimizations based on OMS balloon measurements in the 1990s (Fig. 9) show the more limited sampling compared to the aircraft, primarily in latitude, but the more extensive vertical coverage. The vertical scale on these plots is potential temperature rather than altitude since this emphasizes the stratospheric overworld more than the tropopause region. The balloon measurements extend up to 900 K (34 km altitude), much higher than the ~550 K (22 km) level that can be reached by aircraft. No other *in situ* platform can fly that high, which is of particular value in the tropics.

The OMS balloon Γ_o and R_o values generally agree with those from the aircraft measurements in similar regions during this time period. In the tropics above 600 K, Γ_o and R_o are nearly constant at values of ~3 and 1.5 years. In the northern extratropics, Γ_o reaches 5 years at 900 K and 40°N and 6 years in a deep region of the polar vortex.

Values of R_o peak at ~1.7 years and are nearly constant above 600 K throughout the extratropics. This is in contrast to model estimates that have peak values in the extratropical lower stratosphere and decreasing values up to 10 hPa (Fritsch et al., 2020). The surface source latitudes have similar features to those from the aircraft measurements in the NH. The tropical lower stratosphere has a layered structure of alternating NH and SH influence (Fig. 9c). There is some indication of this in the aircraft data as well but the averaging over all seasons shown in Fig. 8c has reduced the amplitude.
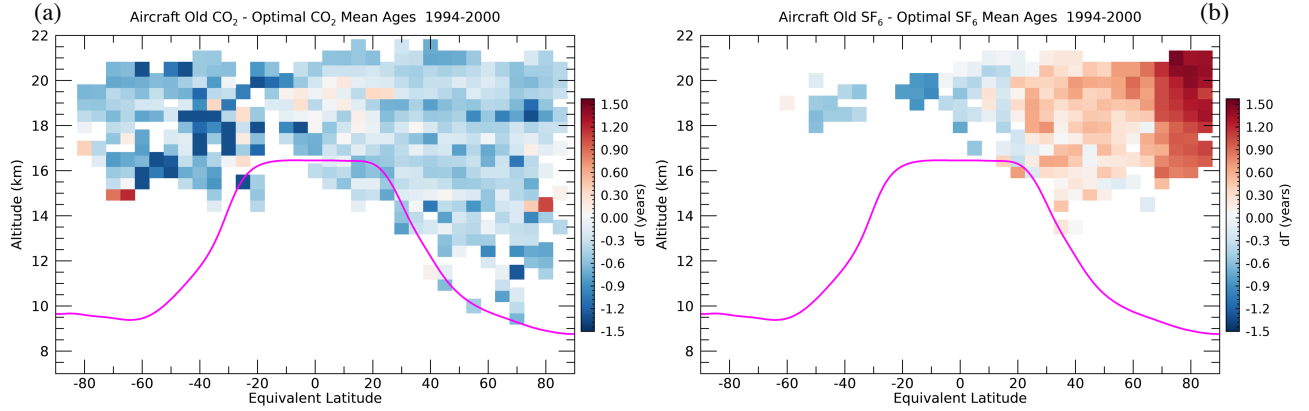
Figure 10. *Gridded average differences between the archived aircraft CO₂ (a) and SF₆ (b) mean ages minus the optimized mean ages in this study. The optimized mean ages are from the single trace gas technique with CO₂ (a) and SF₆ (b) in order to maximize the number of comparison data points for each trace gas. Grid spacing is the same as in Fig. 8.*

Similar to the comparisons in Fig. 7, we can also compare the differences in the spatial distributions of Γ_o with Γ_{SF6} and Γ_{CO2} (Fig. 10). In the comparisons with Γ_{CO2} (Fig. 10a), most locations have a difference of -0.3 to -0.5 years, which represents the transport time between a source region at the tropopause for Γ_{CO2} and the surface for Γ_o. There are some locations with larger differences of -1 year, especially in the SH. The region of these larger age differences in the SH coincides with where Γ_o values are ~1-3 years and the surface source latitudes have SH influence (Fig. 8). The most negative differences were from measurements taken in October (not shown) which has a similar latitudinal dependence in χ_{CO2} as in November (Fig. 2b). At this time of year, a SH surface source results in larger χ_{CO2} values compared to the Mauna Loa-Samoa average and thus a relatively older Γ compared to assuming only a tropical source.

The Γ_{SF6} values are only younger than Γ_o in the tropics and southern midlatitudes (Fig. 10b). The tropics have the youngest mean ages and thus the smallest correction for SF₆ so as with CO₂, the archived mean ages will be younger in this region due to the tropopause vs. surface boundary conditions. In the northern extratropics the mesospheric loss of SF₆ and subsequent old age bias overcomes the 3-6 month negative age bias due to the tropopause versus

surface source region difference resulting in positive mean age differences of up to 1.5 years. This distribution of old age bias generally follows that from the model output of Garny et al. (2024) which was the source of the age bias estimates used in our optimization.

635 *4.2 2020s*

Only in recent years have simultaneous measurements in the stratospheric overworld of the four trace gases utilized in the optimization become available again. This is an unfortunate gap in the monitoring of the stratospheric circulation over the past two decades. With the DCOTSS and SABRE aircraft missions as well as AirCore balloon

640 flights, we now have the ability to calculate age of air from *in situ* measurements in the current stratosphere. The new measurements were the inspiration for this study since a consistent technique is necessary to compare the old and new measurements and age of air. Here we briefly describe the derived mean ages, which have not previously been published from this data, and other transport quantities from the three measurement campaigns in the 2020s. A follow up study will examine the differences between the 1990s and 2020s ages in detail. Briefly, the main

645 differences are younger mean ages at nearly every χ_{N2On} value for the 2020s compared to the 1990s, especially when comparing the aircraft mission data. The younger mean ages are highly suggestive of a strengthened Brewer-Dobson circulation (BDC) over the past two decades.

The distributions of $\Gamma_o - \chi_{N2On}$ for the three different mission data sets are compact and agree well on average, with

650 slightly older Γ_o from AirCore primarily from the winter sampling (Fig. 11). The summer average AirCore mean ages agree within uncertainties with the DCOTSS mission which took place during the NH summer. The distribution of Γ_o in latitude and theta shows the different sampling between the three missions (Fig. 12). DCOTSS used the ER-2 and focused on the summer NH stratosphere which resulted in sampling of relatively young Γ_o up to nearly 500 K and at all latitudes. SABRE used the WB-57 and took place in NH winter with a focus on the polar

655 region where relatively old Γ_o were sampled, although only SF$_6$ was measured during this mission. AirCore uses balloons flown predominantly from Boulder, CO but in various seasons with the oldest Γ_o above 500 K in the midlatitudes. Distributions of R_o and surface source latitudes for each mission are shown in the supplement (Figs. S12, S13).

660
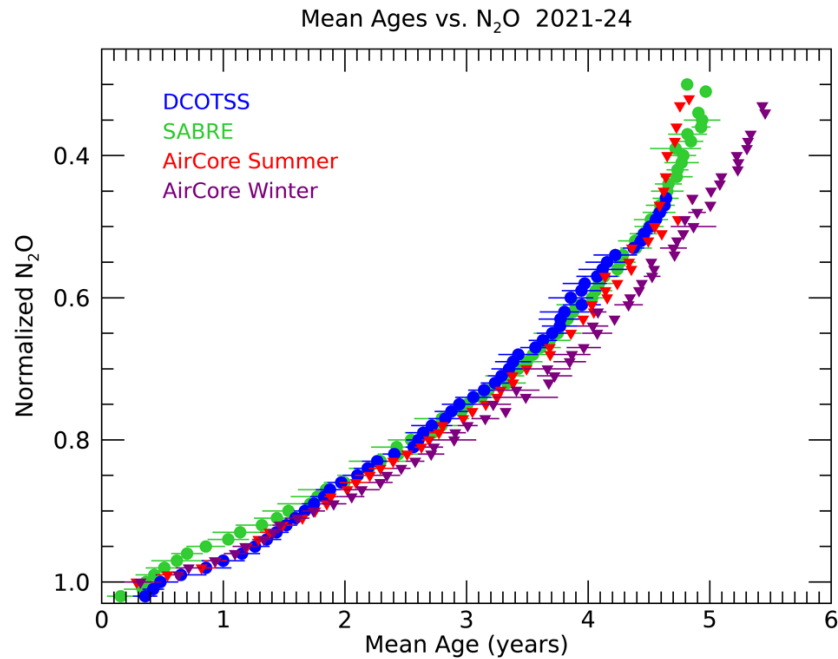
Figure 11. *Distributions of mean age vs. normalized N_2O from DCOTSS (blue) which took place during the summer, SABRE (green) which took place during the winter, and AirCore (red for summer, purple for winter) measurements. The latitude and potential temperature sampled ranges of each mission are shown in Fig. 12.*

665   NOAA's AirCore program is ongoing, and is likely to expand to different latitudes as new recovery techniques for this system are developed, but regardless is a valuable addition to the monitoring of the stratospheric circulation. It is unclear what future aircraft missions will occur with the requisite payload to use this optimization technique and calculate age of air. However, it is unlikely that any period of aircraft sampling of the stratosphere from pole to pole as in the 1990s will occur again.

670
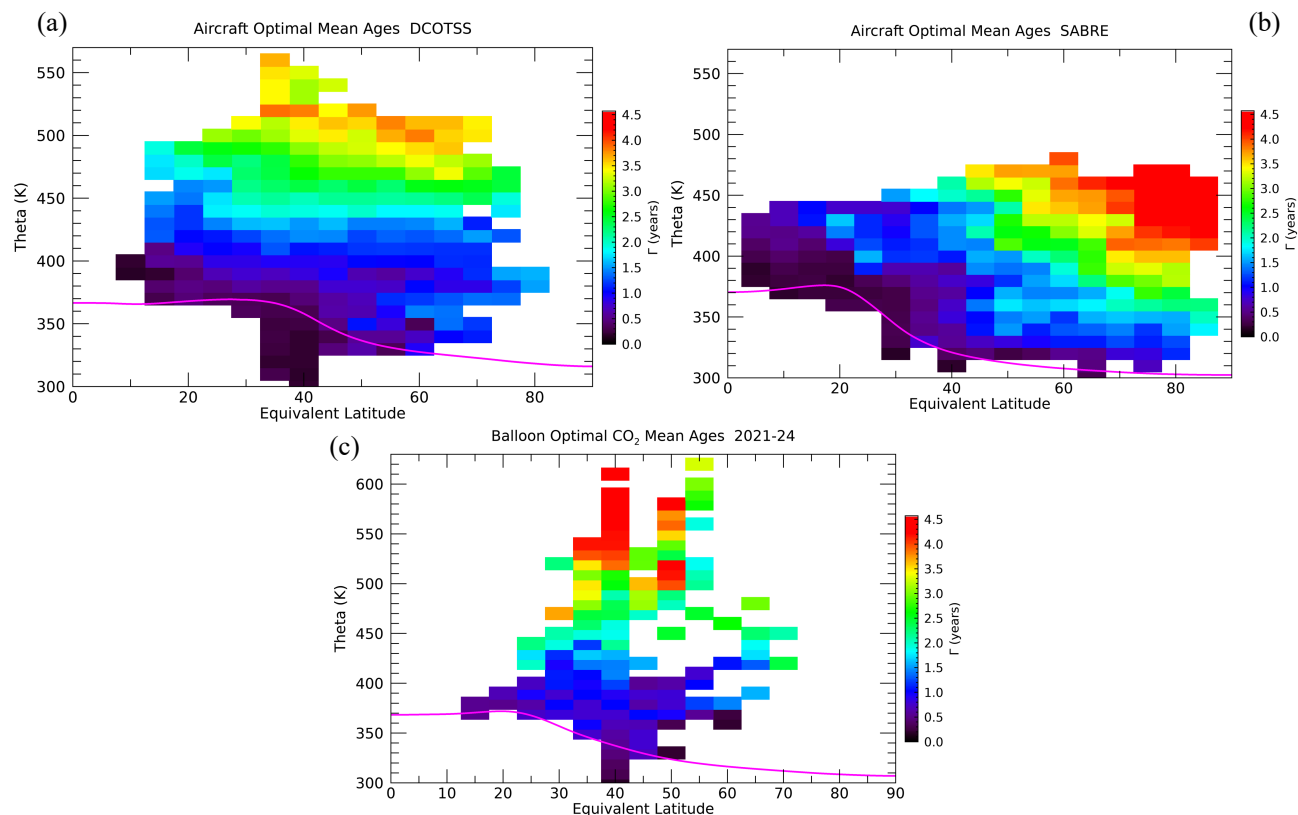
Figure 12. *Equivalent latitude vs. potential temperature distributions of mean age from the DCOTSS (a), SABRE (b) and AirCore (c) missions. Note that the mean age scale and latitude range are different from Figs. 8 and 9 to emphasize the sampled region during these missions. Grid spacing is the same as in Fig. 9.*

5 Summary and Discussion

In this study we describe and demonstrate a new technique to calculate the first and second moments of the age of air distribution as well as surface source latitudes based on aircraft and balloon *in situ* measurements of SF_6, CO_2, CH_4 and N_2O throughout the upper troposphere, lowermost stratosphere and stratospheric overworld. This technique depends crucially on the recent quantification of the time dependent bias in SF_6-derived mean age due to mesospheric loss by Garny et al. (2024) and the NOAA Greenhouse Gas MBL Reference product (Lan et al., 2023) as a time and latitudinally varying surface source for each of the trace gases mentioned above. The main advantages of this new technique are:

1) The use of multiple trace gases allows a single, optimized age of air estimate to be found for each measurement location while minimizing the impact of various uncertainties associated with age of air from single trace gases.

2) Allows the calculation of age of air from the upper troposphere through the stratosphere.

690   3) Flexibility to utilize measurements from different instruments and platforms across decades and account for calibration offsets.

The technique we use is based on the convolution method of estimating age of air and builds on studies such as Bönisch et al. (2009), Ray et al. (2017), Leedham Elvidge et al. (2018) and Ray et al. (2022). One of the primary

695   aspects of how we define the age of air is that it is from the Earth's surface rather than the tropopause as has been commonly used in previous studies. The main reason we choose to use the Earth's surface is that this is where we have long-term measurements of the trace gases used here, which is necessary for any age of air calculation. Of course, all age of air studies have used surface measurements to generate a source region time series for the trace gas(es) of interest, but for those that used the tropopause as a source region, assumptions about how surface trace

700   gas time series translate to the tropopause need to be made.

There are benefits and complications to the choice of the surface as the age of air source region. Complications include (1) significant latitudinal gradients in most trace gases that are in growth, which makes defining a single source region time series difficult, and (2) conceptualizing what age of air from the surface means compared to the more traditional age since an air parcel passes through the tropopause. We address the first complication by

705   partitioning the surface source region time series of each trace gas into two parts, one averaged over all tropical latitudes similar to the standard Mauna Loa-Samoa average (e.g. Boering et al., 1996; Andrews et al., 2001) and a second part averaged over 10° latitude bins from 60°S-60°N that is a free parameter in the calculation (e.g. Ray et al., 2022). The latitudinally varying surface time series is only considered as a source region for the youngest ages

710   of air, on the order of months, primarily because for older ages the measured trace gases lose sensitivity to the surface latitudinal gradients due to mixing. In other words, unlike an idealized tracer in a model that can be emitted and tagged from a certain surface latitude and followed throughout any trajectory and time scale in the atmosphere (e.g. Orbe et al., 2015), real trace gas measurements can only be identified as having been emitted from a certain surface latitude range for a limited time. Conceptually, this means most of the ages in the age spectra in our

715   calculation are from a tropical average surface source similar to that from almost every previous age of air study but without any assumed constant transport time from the surface to the tropopause. The youngest ages in the age spectra have a flexible surface source latitude that allows us to utilize any latitudinal emission information that persists in the measured trace gases.

720   Thus, the complications from the use of the surface as a source region can be turned into a benefit in that additional transport information can be obtained from the trace gas measurements. This benefit is only realized with the use of multiple trace gases since any single trace gas can have too many ambiguities in surface sources combined with transport time scales to constrain the latitudinal source region. The more *in situ* trace gas measurements are available, the more potential there is to constrain the surface source region (e.g. Ray et al., 2022). However, most

725   aircraft and balloon *in situ* payloads have not included instruments that measured more than the four age of air trace gases considered here and often only one or two were measured.

Further benefits of a surface source region include consistency with age of air from CCM output and the ability to calculate age of air at any location in the atmosphere. This last benefit applies primarily to locations in the upper troposphere and above since the shortest transport time scales in the troposphere (days to weeks) require a range of shorter-lived trace gases to define (e.g. Luo et al., 2018). A single technique to calculate age of air in the upper troposphere, tropopause region, lowermost stratosphere and stratospheric overworld can provide new insight into transport in these regions and connect various airborne measurements with different sampling limitations.

A further unique aspect of this study is the offset ensemble as part of the optimization procedure. The assumption behind this technique is that there are many uncertainties in calculating the age of air that are not accounted for in the measurement errors alone. The additional sources of uncertainty can be identified and added together to create a total uncertainty that can be quite large (e.g. Engel et al., 2008). But the offsetting of individual trace gases is a method to identify systematic errors that can often be attributed to a specific issue, such as the SF_6 calibration during the SOLVE mission in the 1990s. The offset optimization accounts for the calibration issue while still calculating mean ages that agree well with values from missions throughout the 1990s. Without the offset method, measurements from SOLVE, for instance, would not be usable in the optimization because there would be no overlap between solutions for SF_6 and CO_2. For other missions and locations there may be a minimal set of overlapping solutions due to an inaccurate assumption of photochemical loss for instance. As long as one of the trace gases, in this case CO_2, requires negligible scaling across essentially all the available measurements then the scaling method can identify and account for systematic errors in the measurements or certain aspects of the age calculation. It may be asked why SF_6 is used at all from the 1990s if the offset values can be large. The benefits of adding SF_6 are many, but primarily it constrains the younger mean ages ($\Gamma < 3$ years) that are not well constrained by CO_2, as shown by the example in Figs. 3 and S8, which then allows better constraint on the ratio of moments.

We demonstrate the technique on the extensive *in situ* measurements from the 1990s and the more limited recent measurements in the 2020s. The 1990s average distributions of mean ages, age spectra width and surface source latitudes from the upper troposphere to the lower stratosphere and nearly pole to pole provide a unique view of average transport at that time. The optimized mean ages calculated here are compared to the archived values previously calculated from CO_2 and SF_6 measurements independently. In many regions the optimized mean ages are similar to the archived values from CO_2, accounting for the surface vs. tropopause source difference. An additional factor that could contribute to older mean ages is the variable surface source latitudes that often result in larger boundary condition CO_2 mixing ratios compared to the Mauna Loa-Samoa average. The optimized mean ages are younger than the previously calculated values from SF_6 everywhere but in the tropics and SH due to the SF_6 mesospheric loss and mean age bias that was not previously accounted for.

The age spectra ratios of moments and surface source latitude distributions from both time periods are unique contributions from this study. The ratios of moments have not been well constrained by observations and the

distributions shown here generally agree well with recently published values from CCM output. The surface source latitudes have a number of interesting features that are beyond the scope of this study to discuss but demonstrate the potential information available from this technique. We also leave comparisons of the results between the two time periods to a follow up study.

The recent aircraft missions and more systematic balloon flights in the stratosphere provided the primary motivation for this study, yet this new data is limited in its ability to detect decadal changes in the stratospheric circulation due to the NH-only sampling. It has been known for quite some time that the average difference in mean age between the tropics and extratropics on an isentrope can reveal the strength of the vertical component of the BDC (Neu and Plumb, 1999; Linz et al., 2017). Yet the last *in situ* measurements in the tropics above 550 K of the four trace gases used in this study to calculate mean ages were made in the 1990s. The result of this lack of tropical measurements is that we have to rely on mean age trends from the somewhat more extensive *in situ* measurements in the NH to infer multi-decadal trends in the BDC (e.g. Engel et al., 2008; 2017). This single hemisphere view is an incomplete picture, partly due to hemispheric shifts in the BDC that can occur on decadal time scales (e.g. Ploeger and Garny, 2022). Satellite measurements of long-lived trace gases can be used to calculate age of air (e.g. Haenel et al., 2015) but thus far no satellite has measured two age tracers such as CO_2 and SF_6 necessary to perform the optimization described here. Thus, *in situ* measurements provide an important complement to satellite measurements and more consistent *in situ* sampling of the tropical and extratropical stratosphere (e.g. Moore et al., 2014) is necessary to better understand and model the ongoing stratospheric circulation changes.

Competing Interests

The contact author has declared that none of the authors has any competing interests.

Acknowledgements

This research was supported in part by NOAA cooperative agreement NA22OAR4320151. An International Space Science Institute (ISSI) project focused on stratospheric age of air led by Hella Garny was helpful in the formulation of this work. The NOAA AirCore program is partially funded by NOAA's Earth's Radiation Budget Initiative, NOAA CPO Climate and CI (grant no. 03-01-07-001). Jack Higgs, Timothy Newberger, Sonja Wolter supported routine AirCore-based flights and analysis for this work. The authors declare no conflicts of interest related to this study. We thank the three anonymous reviewers for their thoughtful comments that have led to improvements in the manuscript.

Data Availability Statement

The processed data supporting this study are available from https://csl.noaa.gov/groups/csl8/modeldata.

Software Availability Statement

The IDL software used to perform the data analysis and make the figures in this study are available from
805   https://csl.noaa.gov/groups/csl8/modeldata.

Author contribution

ER designed and carried out the calculations and wrote the manuscript. FM provided measurement data and
810   conceptual support of the study. HG provided model output and conceptual support. EH, BH, GD, DN, JE, SW, JP,
BD, BB, JL and CS provided measurement data.

References

815   Abalos, M., Calvo, N., Benito-Barca, S., Garny, H., Hardiman, S. C., Lin, P., Andrews, M. B., Butchart, N., Garcia,
R., Orbe, C., Saint-Martin, D., Watanabe, S., and Yoshida, K., The Brewer-Dobson circulation in CMIP6,
Atmos. Chem. Phys., 21, 13571-13591, doi:10.5194/acp-21-13571-2021, 2021.

Andrews, A. E., Boering, K. A., Daube, B. C., Wofsy, S. C., Hintsa, E. J., Weinstock, E. M., and Bui, T. P.,
Empirical age spectra for the lower tropical stratosphere from in situ observations of CO_2: Implications for
820   stratospheric transport, J. Geophys. Res., 104, 26,581-26,595, 1999.

Andrews, A. E., Boering, K. A., Daube, B. C., Wofsy, S. C., Loewenstein, M., Jost, H., Podolske, J. R., Webster, C.
R., Herman, R. L., Scott, D. C., Flesch, G. J., Moyer, E. J., Elkins, J. W., Dutton, G. S., Hurst, D. F., Moore, F.
L., Ray, E. A., Romashkin, P. A., and Strahan, S. E., Mean ages of stratospheric air derived from in situ
observations of CO_2, CH_4, and N_2O, J. Geophys. Res., 106, 32,295-32,314, 2001.

825   Baier, B., Sweeney, C., Newberger, T., Higgs, J., Wolter, S., and NOAA Global Monitoring Laboratory, NOAA
AirCore atmospheric sampling system profiles (Version 20230831) [Data set], NOAA GML,
https://doi.org/10.15138/6AV0-MY81, 2021.

Birner, B., Chipperfield, M. P., Morgan, E. J., Stephens, B. B., Linz, M., Feng, W., Wilson, C., Bent, J. D., Wofsy,
S. C., Severinghaus, J., and Keeling, R. F., Gravitational separation of Ar/N_2 and age of air in the lowermost
830   stratosphere in airborne observations and a chemical transport model, Atmos. Chem. Phys., 20, 12391-12408,
doi:10.5194/acp-20-12391-2020, 2020.

Bischof, W., Borchers, R., Fabian, P., and Kruger, B. C., Increased concentration and vertical distribution of carbon
dioxide in the stratosphere, Nature, 316, 708-710, 1985.

Bönisch, H., Engel, A., Curtius, J., Birner, T., and Hoor, P., Quantifying transport into the lowermost stratosphere
835   using simultaneous in-situ measurements of SF_6 and CO_2, Atmos. Chem. Phys., 9, 5905-5909, 2009.

Boering, K. A., Wofsy, S. C., Daube, B. C., Schneider, H. R., Loewenstein, M., Podolske, J. R., and Conway, T. J., Stratospheric mean ages and transport rates from observations of carbon dioxide and nitrous oxide, Science, 274, 1340-1343, 1996.

Boucher, O., Friedlingstein, P., Collins, B., and Shine, K. P., The indirect global warming potential and global temperature change potential due to methane oxidation, Environ. Res. Lett., 4, doi:10.1088/1748-9326/4/4/044007, 2009.

Chabrillat, S., Vigouroux, C., Christophe, Y., Engel, A., Errera, Q., Minganti, D., Monge-Sanz, B. M., Segers, A., and Mahieu, E., Comparison of mean age of air in five reanalyses using the BASCOE transport model, Atmos. Chem. Phys., 18, 14175-14735, doi:10.5194/acp-18-14175-2018, 2018.

Daniel, J. S., Schauffler, S. M., Pollock, W. H., Solomon, S., Weaver, A., Heidt, L. E., Garcia, R. R., Atlas, E. L., and Vedder, J. F., On the age of stratospheric air and inorganic chlorine and bromine release, J. Geophys. Res., 101, 16,757-16,770, 1996.

Daube, B. C., Boering, K. A., Andrews, A. E., and Wofsy, S. C., High-precision fast-response airborne CO_2 analyzer for in situ sampling from the surface to the middle atmosphere, J. Atmos. Ocean Tech., 19, 1532-1543, 2002.

Diallo, M., Legras, B., and Chedin, A., Age of stratospheric air in the ERA-Interim, Atmos. Chem. Phys., 12, 12133-12154, doi:10.5194/acp-12-12133-2012, 2012.

Dietmuller, S., et al., Quantifying the effect of mixing on the mean age of air in CCMVal-2 and CCMI-1 models, Atmos. Chem. Phys., 18, 6699-6720, doi:10.5194/acp-18-6699-2018, 2018.

Ehhalt, D. H., Rohrer, F., Blake, D. R., Kinnison, D. E., and Konopka, P., On the use of nonmethane hydrocarbons for the determination of age spectra in the lower stratosphere, J. Geophys. Res., 112, doi:10.1029/2006JD007686, 2007.

Elkins, J. W., et al., Airborne gas chromatograph for in situ measurements of long-lived species in the upper troposphere and lower stratosphere, Geophys. Res. Lett, 23, 347-350, 1996.

Engel, A., Mobius, T., Bönisch, H., Schmidt, U., Heinz, R., Levin, I., Atlas, E. Aoki, S., Nakazawa, T., Sugawara, S., Moore, F., Hurst, D., Elkins, J., Schauffler, S., Andrews, A., and Boering, K., Age of stratospheric air unchanged within uncertainties over the past 30 years, Nature Geosci., 2, 28-31, doi:10.1038/ngeo388, 2008.

Engel, A., Boenisch, H., Ullrich, M., Sitals, R., Membrive, O., Danis, F., and Crevoisier, C., Mean age of stratospheric air derived from AirCore observations, Atmos. Chem. Phys., 17, 6825-6838, doi:10.5194/acp-17-6825-2017, 2017.

Etheridge, D. M., Steele, L. P., Francey, R. J., and Langenfelds, R. L., Atmospheric methane between 1000 A.D. and present: Evidence of anthropogenic emissions and climatic variability, J. Geophys. Res., 103, 15,979-15,993, 1998.

Fritsch, F., Garny, H., Engel, A., Bönisch, H., and Eichenger, R., Sensitivity of age of air trends to the derivation method for non-linear increasing inert SF_6, Atmos. Chem. Phys., 20, 8709-8725, doi:10.5194/acp-20-8709-2020, 2020.

Garny, H., Eichinger, R., Laube, J. C., Ray, E. A., Stiller, G. P., Bönisch, H., and Saunders, L.: Correction of
stratospheric age-of-air derived from SF_6 for the effect of chemical sinks, EGUsphere [preprint],
https://doi.org/10.5194/egusphere-2023-1862, 2024.

875 Haenel, F. J., Stiller, G. P., von Clarmann, T., Funke, B., Eckert, E., Glatthor, N., Grabowski, U., Kellmann, S.,
Kiefer, M., Linden, A., and Reddmann, T., Reassessment of MIPAS age of air trends and variability, Atmos.
Chem. Phys., 15, 13161-13176, doi:10.5194/acp-15-13161-2015, 2015.

Hall, T. M., and Plumb, R. A., Age as a diagnostic of stratospheric transport, J. Geophys. Res., 99, 1059-1070, 1994.

Hall, T. M., and Waugh, D. W., Influence of nonlocal chemistry on tracer distributions: Inferring the mean age of air
880 from SF_6, J. Geophys. Res., 103, 13,327-13,336, 1998.

Hall, T. M., Waugh, D. W., Boering, K. A., and Plumb, R. A., Evaluation of transport in stratospheric models, J.
Geophys. Res., 104, 18,815-18,839, 1999.

Hauck, M., Fritsch, F., Garny H., and Engel, A., Deriving stratospheric age of air spectra using an idealized set of
chemically active trace gases, Atmos. Chem. Phys., 19, 5269-5291, doi:10.5194/acp-19-5269-2019, 2019.

885 Hauck, M., Bönisch, H., Hoor, P., Keber, T., Ploeger, F., Schuck, T. J., and Engel, A., A convolution of
observational and model data to estimate age of air spectra in the northern hemispheric lower stratosphere,
Atmos. Chem. Phys., 20, 8763-8785, doi:10.5194/acp-20-8763-2020, 2020.

Herman, R. L., Ray, E. A., Rosenlof, K. H., Bedka, K. M., Schwartz, M. J., Read, W. G., Troy, R. F., Chin, K.,
Christensen, L. E., Fu, D., Stachnik, R. A., Bui, T. P., and Dean-Day, J. M.: Enhanced stratospheric water vapor
890 over the summertime continental United States and the role of overshooting convection, Atmos. Chem. Phys.,
17, 6113–6124, https://doi.org/10.5194/acp- 17-6113-2017, 2017.

Hintsa, E. J., et al., UAS Chromatograph for Atmospheric Trace Species (UCATS) – a versatile instrument for trace
gas measurements on airborne platforms, Atmos. Meas. Tech., 14, 6795-6819, doi:10.5194/amt-14-2021, 2021.

Holzer, M. and Waugh, D. W., Interhemispheric transit time distributions and path-dependent lifetimes constrained
895 by measurements of SF_6, CFCs and CFC replacements, Geophys. Res. Lett., 42, doi:10.1002/2015GL064172,
2015.

Kida, H., General circulation of air parcels and transport characteristics derived from a hemispheric GCM part 2.
Very long-term motions of air parcels in the troposphere and stratosphere, J. Meteo. Soc. Japan, 61, 510-523,
1983.

900 Lan, X., Tans, P., Thoning, K., and NOAA Global Monitoring Laboratory, NOAA Greenhouse Gas Marine
Boundary Layer Reference, [data set], NOAA GML, doi:10.15138/DVNP-F961, 2023.

Leedham Elvidge, E., Bönisch, H., Brenninkmeijer, C. A. M., Engel, A., Fraser, P. J., Gallacher, E., Langenfelds,
R., Muhle, J., Oram, D. E., Ray, E. A., Ridley, A. R., Rockmann, T., Sturges, W. T., Weiss, R. F., and Laube, J.
C., Evaluation of stratospheric age of air from CF4, C2F6, C3F8, CHF3, HFC-125, HFC-227ea and SF6;
905 implications for the calculations of halocarbon lifetimes, fractional release factors and ozone depletion potentials,
Atmos. Chem. Phys., 18, 3369-3385, doi:10.5194/acp-18-3369-2018, 2018.

Li, J., Baier, B. C., Moore, F., Newberger, T., Wolter, S., Higgs, J., Dutton, G., Hintsa, E., Hall, B., and Sweeney,
C., A novel, cost-effective analytical method for measuring high-resolution vertical profiles of stratospheric trace

gases using a gas chromatograph coupled with an electron capture detector, Atmos. Meas. Tech., 16, 2851-2863, doi:10.5194/amt-16-2851-2023, 2023.

Linz, M., Plumb, R. A., Gerber, E. P., Haenel, F. J., Stiller, G., Kinnison, D. E., Ming, A., and Neu, J. L., The strength of the meridional overturning circulation of the stratosphere, Nat. Geosci., 10, 663-668, doi:10.1038/NGEO3013, 2017.

Loeffel, S., Eichinger, R., Garny, H., Reddmann, T., Fritsch, F., Versick, S., Stiller, G., and Haenel, F., The impact of sulfur hexafluoride (SF_6) sinks on age of air climatologies and trends, Atmos. Chem. Phys., 22, 1175-1193, doi:10.5194/acp-22-1175-2022, 2022.

Loewenstein, M., Jost, H., Grose, J., Eilers, J., Lynch, D., Jensen, S., and Marmie, J., Argus: a new instrument for the measurement of the stratospheric dynamical tracers, N_2O and CH_4, Spec. Acta Part A: Mol. Biomol. Spec., 58, 2329-2345, doi:10.1016/S1386-1425(02)00048-3, 2001.

Luo, Z. J., et al., Use of airborne in situ VOC measurements to estimate transit time spectrum: An observation-based diagnostic of convective transport, Geophys. Res. Lett., 45, 13,150-13,157, doi:10.1029/2018GL080424, 2018.

Meinshausen, M., et al., Historical greenhouse gas concentrations for climate modelling (CMIP6), Geosci, Model Dev., 10, 2057-2116, doi:10.5194/gmd-10-2057-2017, 2017.

Moore, F. L., Elkins, J. W., Ray, E. A., Dutton, G. S., Dunn, R. E., Fahey, D. W., McLaughlin, R. J., Thompson, T. L., Romashkin, P. A., Hurst, D. F., and Wamsley, P. R., Balloonborne in situ gas chromatograph for measurements in the troposphere and stratosphere, J. Geophys. Res., 108, doi:10.1029/2001JD000891, 2003.

Moore, F. L., Ray, E. A., Rosenlof, K. H., Elkins, J. W., Tans, P., Karion, A., and Sweeney, C., A cost-effective trace gas measurement program for long-term monitoring of the stratospheric circulation, Bull. Amer. Meteo. Soc., 147, doi:10.1175/BAMS-D-12-00153.1, 2014.

Neu, J. L., and Plumb, R. A., Age of air in a "leaky pipe" model of stratospheric transport, J. Geophys. Res., 104, 19,243-19,255, 1999.

Orbe, C., Waugh, D. W., and Newman, P. A., Air-mass origin in the tropical lower stratosphere: The influence of Asian boundary layer air, Geophys. Res. Lett., 42, doi:10.1002/2015GL063937, 2015.

Ploeger, F., Abalos, M., Birner, T., Konopka, P., Legras, B., Muller, R., and Riese, M., Quantifying the effects of mixing and residual circulation on trends of stratospheric mean age of air, Geophys. Res. Lett., 42, 2047-2054, doi:10.1002/2014GL062927, 2014.

Ploeger, F., and Birner, T., Seasonal and inter-annual variability of lower stratospheric age of air spectra, Atmos. Chem. Phys., 16, 10195-10213, doi:10.5194/acp-16-10195-2016, 2016.

Ploeger, F., Legras, B., Charlesworth, E., Yan, X., Diallo, M., Konopka, P., Birner, T., Tao, M., Engel, A., and Riese, M., How robust are stratospheric age of air trends from different reanalyses?, Atmos. Chem. Phys., 19, 6085-6105, doi:10.5194/acp-19-6085-2019, 2019.

Ploeger, F., and Garny, H., Hemispheric asymmetries in recent changes in the stratospheric circulation, Atmos. Chem. Phys., 22, 5559-5576, doi:10.5194/acp-22-5559-2022, 2022.

Plumb, R. A., and Ko, M. K. W., Interrelationships between mixing ratios of long-lived stratospheric constituents, J. Geophys. Res., 97, 10,145-10,156, 1992.

Podglajen, A. and Ploeger, F., Retrieving the age of air spectrum from tracers: principle and method, Atmos. Chem. Phys., 19, 1767-1783, doi:10.5194/acp-19-1767-2019, 2019.

Ray, E. A., et al., Improving stratospheric transport trend analysis based on SF_6 and CO_2 measurements, J. Geophys. Res., 119, doi:10.1002/2014JD021802, 2014.

950   Ray, E. A., Moore, F. L., Elkins, J. W., Rosenlof, K. H., Laube, J. C., Rockmann, T., Marsh, D. R., and Andrews, A. E., Quantification of the SF6 lifetime based on mesospheric loss measured in the stratospheric polar vortex, J. Geophys. Res., 122, doi:10.1002/2016JD026198, 2017.

Ray, E. A., Atlas, E. L., Schauffler, S., Chelpon, S., Pan, L., Bönisch, H., and Rosenlof, K. R., Age spectra and other transport diagnostics in the North American monsoon UTLS from SEAC[4]RS in situ trace gas measurements,

955   Atmos. Chem. Phys., 22, 6539-6558, doi:10.5194/acp-22-6539-2022, 2022.

Schmidt, U. and Khedim, A., In situ measurements of carbon dioxide in the winter Arctic vortex and at midlatitudes: An indicator of the 'age' of stratospheric air, Geophys. Res. Lett., 4, 763-766, 1991.

Schoeberl, M. R., Sparling, L. C., Jackman, C. H., and Fleming, E. L., A Lagrangian view of stratospheric trace gas distributions, J. Geophys. Res., 105, 1537-1552, 2000.

960   Schoeberl, M. R., Douglass, A. R., Polansky, B., Boone, C., Walker, K. A., Bernath, P., Estimation of stratospheric age spectrum from chemical tracers, J. Geophys. Res., 110, D21303, doi:10.1029/2005JD006125, 2005.

Shindell, D. T., Fuglestvedt, J. S., and Collins, W. J., The social cost of methane: theory and applications, Faraday Discuss., 200, 429-451, doi:10.1039/c7fd00009j, 2017.

Strahan, S. E., et al., Using transport diagnostics to understand chemistry climate model ozone simulations, J.

965   Geophys. Res., 116, doi:10.1029/2011JD015360, 2011.

Volk, C. M., Elkins, J. W., Fahey, D. W., Dutton, G. S., Gilligan, J. M., Loewenstein, M., Podolske, J. R., Chan, K. R., and Gunson, M. R., Evaluation of source gas lifetimes from stratospheric observations, J. Geophys. Res., 102, 25,543-25,564, 1997.

Waugh, D. W., et al., Three-dimensional simulations of long-lived tracers using winds from MACCM2, J. Geophys.

970   Res., 102, 21,493-21,513, 1997.

Waugh, D. W. and Hall, T. M., Age of stratospheric air: Theory, observations, and models, Rev. Geophys., 40, doi:/10.1029/2000RG00101, 2002.

Waugh, D. W., et al., Tropospheric SF6: Age of air from the Northern Hemisphere midlatitude surface, J. Geophys. Res., 118, doi:10.1002/jgrd.50848, 2013.

975   Webster, C. R., May, R. D., Trimble, C. A., Chave, R. G., and Kendall, J., Aircraft (ER-2) laser infrared absorption spectrometer (ALIAS) for in-situ stratospheric measurements of HCl, N_2O, CH_4, NO_2, and HNO_3, Applied Optics, 33, 454-472, 1994.

Webster, C. R., et al., Quantum-cascade laser measurements of stratospheric methane and nitrous oxide, Applied Optics, 40, 321-326, 2001.

980   Woodbridge, E. L., Elkins, J. W., Fahey, D. W., Heidt, L. E., Solomon, S., Baring, T. J., Gilpin, T. M., Pollock, W. H., Schauffler, S. M., Atlas, E. L., Loewenstein, M., Podolske, J. R., Webster, C. R., May, R. D., Gilligan, J. M., Montzka, S. A., Boering, K. A., and Salawitch, R. J., Estimates of total organic and inorganic chlorine in the

lower stratosphere from in situ and flask measurements during AASE II, J. Geophys. Res., 100, 3057-3064, 1995.

985   Yan, X., Konopka, P., Hauck, M., Podglajen, A., and Ploeger, F., Asymmetry and pathways of inter-hemispheric transport in the upper troposphere and lower stratosphere, Atmos. Chem. Phys., 21, 6627-6645, doi:10.5194/acp-22-6627-2021, 2021.